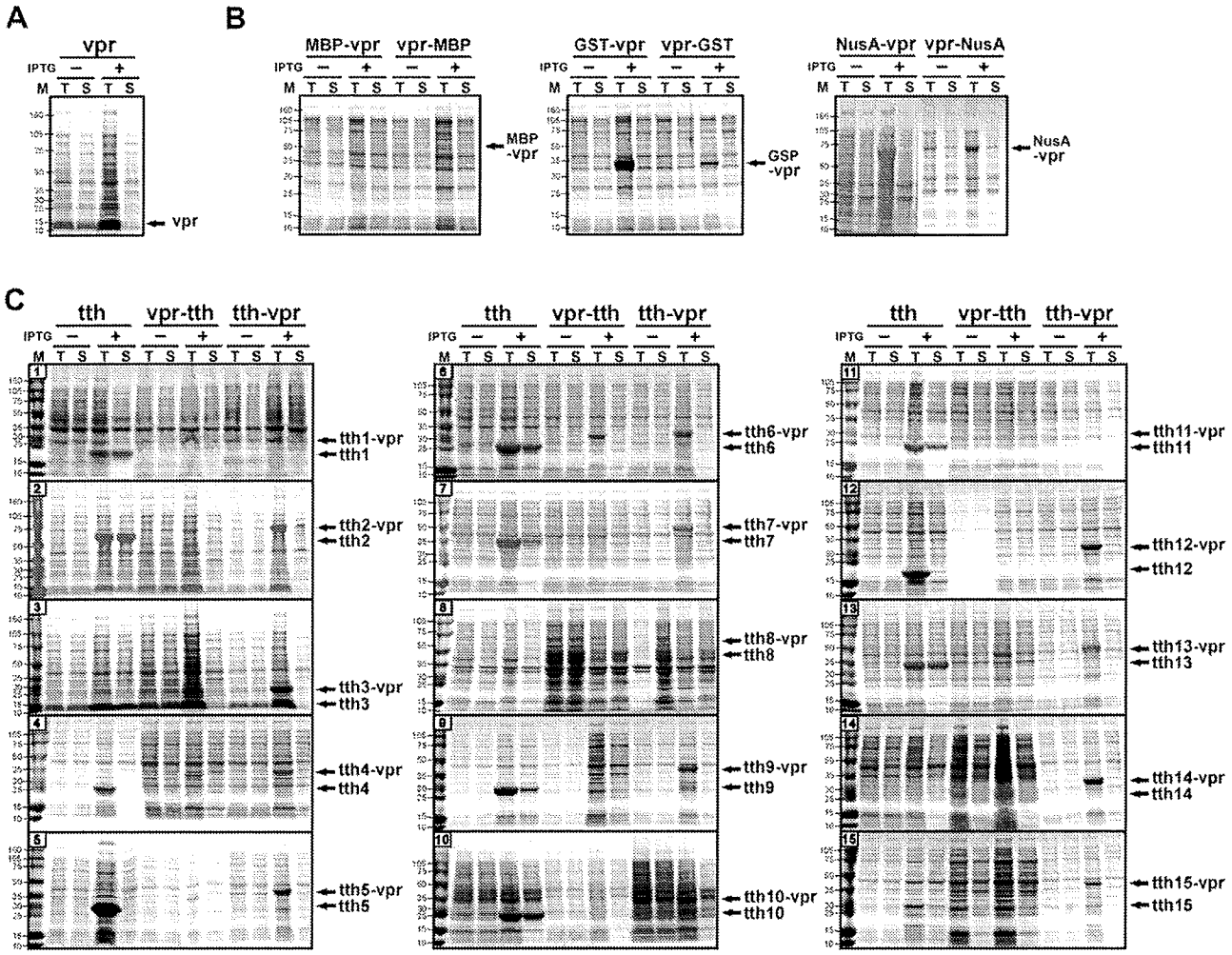

Fig. 2. Expression profile of tag protein-fused Vpr with (+) or without (–) induction by IPTG. Based on calculated molecular weights, the positions of expected proteins are marked by arrows along the right edge of each gel. (A) Expression profiles of tag-free Vpr. (B) Expression profiles of MBP-fused Vpr, GST-fused Vpr, and NusA-fused Vpr. (C) Expression profiles of individual *T. th.* protein candidates alone (tth) and when fused with Vpr at the C terminus (vpr–tth) or at the N terminus (tth–vpr). The number indicated in the box in the upper left corner of each gel corresponds to the number used for the candidate tth gene listed in Table 1. Gel columns indicate molecular weight markers (in kDa) (M), total lysate (T), and supernatant (S).

Table 1
Selected candidates of protein tags from *T. th.*

Name in this study	Locus tag in genome	Functional feature	M_W (kDa)	PDB ID	Resolution (Å)
tth1	TTHA0132	Conserved hypothetical protein	16.9	2dx6	1.78
tth2	TTHA0271	Molecular chaperon, GroEL	57.9	1wf4	2.80
tth3	TTHA0281	UPF0150 family protein	9.8	2dsy	1.90
tth4	TTHA0341	Molybdopterin biosynthesis enzyme MoaB	17.8	2is8	1.64
tth5	TTHA1053	Conserved hypothetical protein	20.7	2cve	1.60
tth6	TTHA1091	Conserved hypothetical protein	17.8	1vgg	1.75
tth7	TTHA1199	Ornithine carbamoyltransferase	33.3	2ef0	2.00
tth8	TTHA1275	C subunit of $V_1 - V_0$ ATPase	36.0	1v9m	1.85
tth9	TTHA1359	Transcriptional regulator	22.4	2zcw	1.50
tth10	TTHA1671	Adenylate kinase	20.7	3cm0	1.80
tth11	TTHA1699	Putative transediting enzyme of tRNA-Syn	16.6	2cx5	1.90
tth12	TTHA1713	Conserved hypothetical protein	14.4	2cu5	1.84
tth13	TTHA1838	Atypical ABC-ATPase, SufC	27.6	2d2f	1.90
tth14	TTHA1897	GidA-related protein	25.9	2cul	1.65
tth15	TTHB192	CRISPR-associated protein	23.8	1wj9	1.90

Expression of Vpr protein with T. th. protein fusion

Because the expression vectors used in this study (pET-47b and pET-47md) (Fig. 1) have the polyhistidine and protease recognition sequences that are absent from the vectors used in the *T. th.* SG project (pET-3a and pET-11a) [28,29], we began our investigation by evaluating the selected *T. th.* proteins in the pET-47b backbone. Our results showed that although all *T. th.* proteins were expressed well, 7 of the 15 *T. th.* proteins (Tth4, Tth5, Tth7, Tth8, Tth12, Tth14, and Tth15) failed to solubilize (Fig. 2C, tth). Because the general

conditions for the expression, such as growth medium, growth temperature (37 °C), and IPTG concentration, were identical to those of the original *T. th.* SG project, the differences in the used expression vectors, especially the presence of a polyhistidine tag and the protease recognition site in the pET-47md backbone, seem to have affected the solubility of the *T. th.* proteins.

Then we tested the expression level and the solubility of *T. th.* tag-fused Vpr. Except for tags Tth1, Tth8, and Tth11, all *T. th.* tags facilitate the expression level of the fusion protein when the *T. th.* proteins had been added at the N terminus of Vpr (Fig. 2C, tth–vpr). However, in the case of C terminus addition, only the Tth6-fused protein among the *T. th.* tag-fused Vpr proteins was expressed well (Fig. 2C, vpr–tth).We found that the Tth2 protein enhanced the solubility of Vpr when Tth2 was added to the N terminus of Vpr (Fig. 2C).

Efficacy of the tag proteins on other insoluble proteins

We investigated the efficacy of *T. th.* tag proteins on other insoluble proteins from primate lentiviruses. Based on the results of *T. th.* alone or *T. th.* in a Vpr fusion form (Fig. 2), seven *T. th.* tags (Tth2, Tth3, Tth6, Tth9, Tth10, Tth11, and Tth13) were introduced to the N terminus of two lentiviral proteins. Three conventional tags were also introduced to this position. One of these proteins, gp41-MSD, is a highly hydrophobic 2.2-kDa peptide that anchors the envelope protein to lipid bilayers [27]. The synthetic peptide of gp41-MSD remains insoluble under the condition of 100% dimethyl sulfoxide (unpublished data). Another protein, Vpx, is a virion-associated 12.9-kDa protein of SIV that plays an important role in nuclear transport of the incoming preintegration complex [26]. Vpr and Vpx are evolutionarily related to each other and have approximately 15% of their primary structures in common. Among the conventional tags, MBP and NusA enhanced the expression level of tag-fused gp41-MSD (Fig. 3A), but the expressed proteins could not be found in the soluble fractions (Fig. 3A). Six *T. th.* tags (Tth2, Tth6, Tth9, Tth10, Tth11, and Tth13) enhanced expression levels when fused at the N terminus (Fig. 3B). Both the Tth2 and Tth10 proteins were partially successful at solubilizing gp41-MSD (Fig. 3B). In the case of Vpx, expression levels were enhanced when fused with NusA, Tth2, Tth3, Tth6, Tth9, Tth10, Tth11, and Tth13, although none of these fusion proteins could be solubilized (data not shown). These results suggest that *T. th.*-tagged proteins can enhance the expression level of insoluble proteins; however, the efficacy depends heavily on the passenger proteins used.

Effect of tag proteins on the function of passenger proteins

It is of interest to know whether fusion of a tag may affect any functions of the fused passenger protein. We attempted to test what effect, if any, the *T. th.* tag-fused Vpr had on the cell cycle, but our efforts at transduction of the purified proteins into the mammalian cells were not too successful. In the case of gp41-MSD, there is no good biological assay because it is a portion of a protein. Therefore, we used GFP as a surrogate reporter for Tth2, Tth6, Tth9, Tth10, Tth11, and Tth13. Most of the tag proteins, such as Tth2, Tth3, Tth6, and Tth9, enhanced expression to levels comparable to those achieved with the conventional tags GST and NusA (Fig. 4A). Moreover, Tth2, Tth10, and Tth13 proteins enhanced the solubility of fused GFPs. The fluorescence-activated cell sorting (FACS) analyses of the fluorescence of the fused GFPs showed that the fluorescent intensity of MBP, GST, Tth11, and Tth13 fused proteins was less than half the intensity of intact GFP (Fig. 4B). As shown in Fig. 4A, both the expression level and solubility of these fusion proteins were similar to those of intact GFP; however, the fusion with these tags reduced the activity of GFP. In the case of Tth2, Tth3, Tth6, Tth9, and Tth10 proteins, the fusion affected the fluorescence of GFP only slightly.

We next examined the stability of the tagged GFPs under denaturing conditions by treating the proteins with GdmHCl (Fig. 4C and D). For the conventional tag proteins, the denaturation profile of GST-fused GFP was nearly identical to that of intact GFP, although for MBP and NusA the normalized fluorescence intensities of the tag-fused proteins were slightly lower than the intensity of intact GFP (Fig. 4C). On the other hand, all denaturation profiles of *T. th.* tag-fused proteins, except for Tth13, were similar to the profile of tag-free GFP (Fig. 4D). These results suggest that the *T. th.* tag proteins do not destabilize the GFP passenger protein. We also observed the endurance of the tag-fused proteins to heat treatment (see Supplemental Fig. 1 in supplementary material), suggesting the possibility of a simple purification protocol employing a heat treatment.

Purification and characterization of tag-fused proteins

To verify whether a large amount of tag protein can be obtained using a *T. th.* tag-mediated system, large-scale expression and purification were performed. Tth2- or Tth10-fused protein was used because these two tags could efficiently solubilize insoluble protein. After induction, the proteins were purified in two steps: using nickel–nitrilotriacetate (Ni–NTA) columns and through size exclusion (Fig. 5A). Despite the good expression, the Tth2–Vpr protein was harder to purify, probably owing to the residual insoluble properties derived from Vpr. Except for the Tth2–Vpr protein, at least 1 mg of pure protein was obtained from a 1-L culture. Meanwhile, because a high concentration of salt improved the solubility of tag-fused proteins, 0.5 M NaCl was added at all of the purification and analysis steps. CD spectra of purified proteins were measured. CD of the Tth2 protein showed the typical pattern of an α-helix-containing protein, which has negative maxima at 209 and 222 nm (Fig. 5B), consistent with the results of crystal structure of Tth2 protein (PDB ID: 1WF4). Other proteins fused with Tth2 proteins, such as Tth2–GFP, Tth2–Vpr, and Tth2–gp41-MSD, also

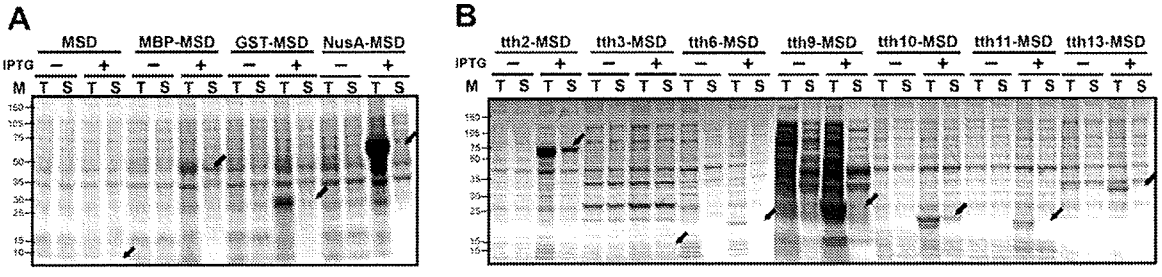

Fig. 3. Efficacy of tag protein for the expression of insoluble protein, gp41-MSD (MSD) from HIV-1. (A) Expression profiles of MSD alone and when fused with each of three conventional tags: MBP, GST, and NusA. (B) Expression profiles of tth-fused MSD. Each arrow indicates the position of the expected molecular weight of the fusion protein. Abbreviations are as defined in Fig. 2.

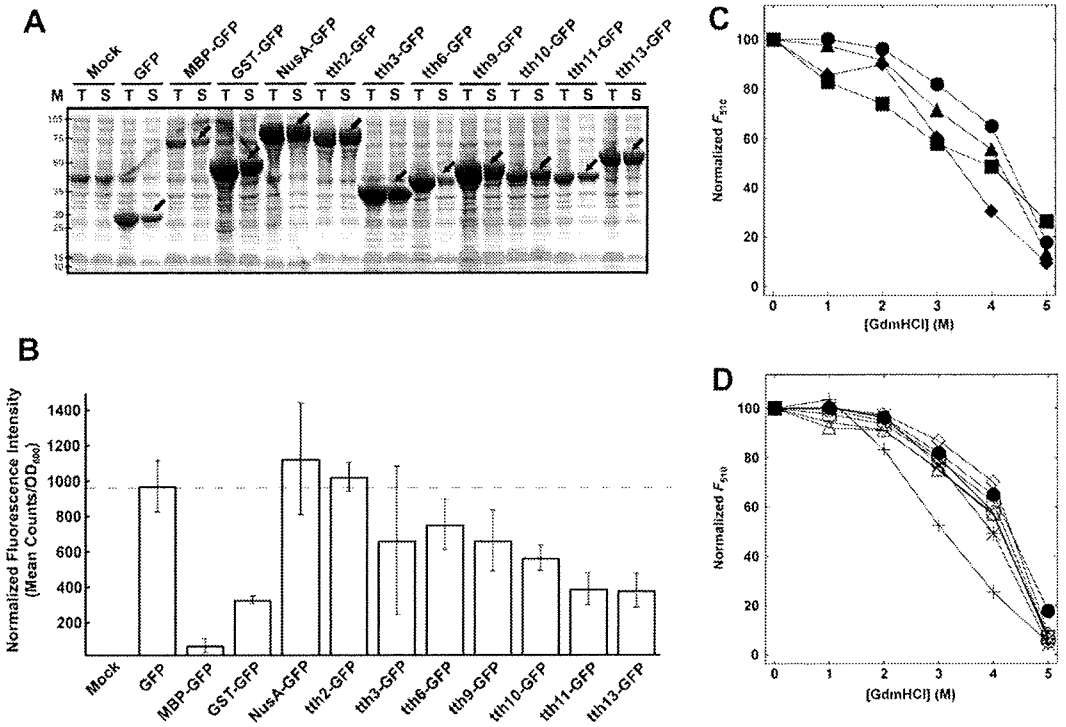

Fig. 4. Properties of tag-fused GFP. (A) Expression profile of tag-fused GFP. All cell extracts were prepared after 5 h exposure to 1 mM IPTG. Based on the calculated molecular weights, the positions of expected proteins are marked by arrows. Abbreviations are as defined in Fig. 2. (B) Fluorescence intensity of tag-fused GFP-expressing *E. coli* cells. The profiles of expression levels of GFP or tag-fused GFPs are the same as those in panel A. The measured mean fluorescence signal was normalized by dividing by the optical density of the culture at 600 nm. The standard deviations were calculated based on the results obtained in more than five independent experiments. (C,D) Residual intensity at 510 nm of proteins fused with conventional tags (C) or tth tags (D) and denatured by GdmHCl. Fluorescence intensities are expressed using nondenatured GFP as 100%. ●, tag-free GFP; ■, MBP-fused GFP; ▲, GST-fused GFP; ♦, NusA-fused GFP; ○, tth2-fused GFP; □, tth3-fused GFP; ◇, tth6-fused GFP; △, tth9-fused GFP; ▽, tth10-fused GFP; *, tth11-fused GFP; +, tth13-fused GFP.

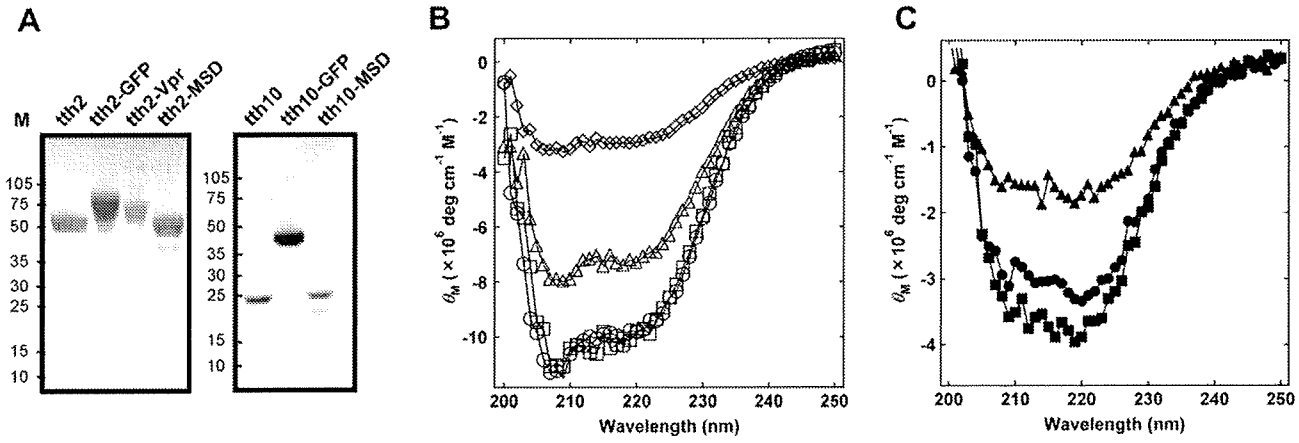

Fig. 5. Purification and secondary structure analyses of tag-fused proteins. (A) SDS–PAGE profile of purified proteins with MSD indicating gp41-MSD. (B) CD spectra of tth2-fused proteins. ○, tth2 alone; □, tth2-fused GFP; △, tth2-fused Vpr; ◇, tth2-fused MSD. (C) CD spectra of tth10-fused proteins. ●, tth10 alone; ■, tth10-fused GFP; ▲, tth10-fused MSD.

have similar negative maxima, suggesting that a considerable number of α-helical structures were present in the tag-fused proteins (Fig. 5B). The intensities of CD spectra for Tth2 and Tth2–GFP proteins were nearly identical, whereas those of Tth2–Vpr and Tth2–gp41-MSD proteins were lower. As for Tth10 and Tth10-fused proteins, the patterns of negative maxima were similar but the intensity of Tth10-fused gp41-MSD was reduced compared with that of Tth10 protein alone. Although it is difficult to explain the decrease in the intensities, the observed decreases may suggest that fusion-driven alterations to the proteins' structures occur.

Discussion

In this study, we used the information on properties of the *T. th.* proteins accumulated during structural genomics studies to produce tag proteins that could facilitate the high production of target proteins. We applied two major criteria for the selection of the candidate tag proteins: high expression level and high solubility. The additional criterion, a high-resolution structure, was employed because this characteristic can facilitate phase determination during X-ray diffraction; the fused tag can be used as a template for molecular replacement. The 15 proteins that

met these criteria were diverse in their functions and structures (Table 1).

We examined the versatility of the selected tag proteins by fusing them to the highly insoluble adaptor protein Vpr. The candidate *T. th.* tag proteins showed themselves to be more effective when placed at the N terminus of Vpr (Fig. 2). The efficacies of the enhancements to protein expression proved to be nearly comparable to—or sometimes better than—those achieved with conventional tag proteins. Thus, the proteins derived from *T. th.* can be used as alternative tag proteins for efficient protein expression. Furthermore, we successfully identified one *T. th.* tag protein, Tth2, that could express Vpr in a soluble form. In addition to Tth2, the Tth10 protein could solubilize the extremely insoluble gp41-MSD (Figs. 2 and 3) more effectively than MBP, GST, or NusA.

When we tested Vpx as the fusion partner, the *T. th.* tag-fused proteins were expressed better than tag-free proteins, although the tagged proteins did not solubilize (data not shown). This apparent difference in solubility could arise from many factors other than the difference of the passenger proteins. One possible factor is the influence of the sequence that links the tag and the passenger protein. Indeed, we observed that some *T. th.* tags became insoluble when fused to a polyhistidine tag in our pET-47 vector (Fig. 2C). Others have observed similar effects of the linker sequence on expression and, possibly, solubility [12–14]. The linker sequence also plays an important role in the crystallization of a tag-fused protein [17]. Therefore, for successful analyses, it seems to be essential that both the fusion tag and linker sequence be carefully selected.

The high crystallization characteristics of *T. th.* proteins may confer additional advantage to this tag system. For this reason, we intended to retain the *T. th.* tag proteins after the purification not only to keep the proteins soluble but also to facilitate their crystallization. Therefore, we estimated the effects that the tag proteins had on the passenger proteins. Our analyses of tag-fused GFPs showed that 7 of the 15 candidate *T. th.* tags did not diminish either the function or the stability of GFP (Fig. 4). Even the considerable effect that the Tth2 protein had on the function of the passenger protein compared favorably with that produced with GST. In contrast, MBP had a considerable negative effect on the function of GFP; it also decreased the expression level of GFP itself. This effect has been reported previously [36]. Our results suggest that *T. th.* tags have similar or milder effects on the function of passenger proteins compared with the effects produced with the conventional tags MBP, GST, and NusA.

We focused mainly on the practical properties of *T. th.* proteins rather than on their biological functions when selecting our candidate tag proteins. Therefore, the two successful candidates identified for Vpr and gp41-MSD in this study have unrelated biochemical properties; Tth2 protein is the molecular chaperon GroEL, and Tth10 protein is the phosphotransferase adenylate kinase (Table 1). Each is known to undergo a conformational change on ligand binding [37–40], a characteristic suggesting that these proteins have flexible structures. In Fig. 5, the molar ellipticities of the fusion proteins, especially those fused with insoluble proteins, were not cumulative against the ellipticity of *T. th.* tag alone. The decrease in the intensities of the *T. th.* tag-fused insoluble proteins, such as Tth2–Vpr, Tth2–gp41-MSD, and Tth10–gp41-MSD, may reflect the structure alternation of the *T. th.* tag proteins for solubilization. There seems to be no severe structural alteration in the passenger protein; the fluorescent intensities of GFP and Tth2- or Tth10-fused GFP were nearly identical (Fig. 4).

In the case of Tth2 protein, the chaperon activity of GroEL may mediate the process of protein-folding and result in the efficient solubilization of the passenger protein [41]. Indeed, coexpression of GroEL/GroES for the production of target proteins in *E. coli* is widely used for the production of correctly folded proteins [42–46]. It has been reported, however, that GroEL from *T. th.* does not have chaperon activity alone [47]. If Tth2 protein acts as a molecular chaperon, endogenous GroES in *E. coli* may function in a coordinate manner during protein synthesis. At this point, we cannot explain the exact mechanism of Tth2-induced solubilization.

In this study, we have used the systematically accumulated data of the structural genomics project of *T. th.* to develop tag proteins useful for protein expression and solubilization. The properties used for the selection of candidate tags, such as high expression level and high solubility, are beneficial but do not necessarily guarantee that the protein will be a successful solubilizing partner. Although different proteins may need different fusion tags to achieve maximum efficacy of expression and solubility, it is noteworthy that the highly hydrophobic gp41-MSD could be solubilized with the use of *T. th.* tag. It is estimated that approximately 30% of all proteins are membrane proteins, and structural analysis of these proteins can be difficult because these proteins are often insoluble. The approach shown here may facilitate their structural analysis. Our preliminary trials of crystallization of *T. th.* tag-fused Vpr and gp41-MSD yielded small crystals. We are interested in determining whether the attached tag protein can facilitate phase determination during X-ray crystallographic analyses, as we have proposed. Moreover, investigation of this type must be useful because the greater the number of effective solubility-enhancing tags we can identify, the better are the chances of understanding the mechanism of solubility enhancement.

Acknowledgments

This work was supported in part by the Program of Founding Research Centers for Emerging and Reemerging Infectious Diseases of the Ministry of Education, Culture, Sports, Science, and Technology (MEXT). We are grateful to the staff members of the Structural Biology Core Facility at the Institute of Biophysics, Chinese Academy of Sciences, for technical assistance. We thank Zhensheng Xie of Proteomic Platform at the Institute of Biophysics, Chinese Academy of Sciences, for identification of proteins with mass spectrometry. We thank Xinyu Wang for assistance with the Pistar instrument. We thank Kunito Yoshiike and Mark Bartlam for a critical reading of the manuscript. We also thank A. M. Menting, an editorial consultant, for preparation of the manuscript.

Appendix A. Supplementary data

Supplementary data associated with this article can be found, in the online version, at doi:10.1016/j.ab.2008.10.050.

References

[1] S.G. Dahl, I. Sylte, Molecular modeling of drug targets: The past, the present, and the future, Basic Clin. Pharmacol. Toxicol. 96 (2005) 151–155.
[2] K. Klumpp, T. Mirzadegan, Recent progress in the design of small molecule inhibitors of HIV RNase H, Curr. Pharm. Des. 12 (2006) 1909–1922.
[3] P. Beltrao, C. Kiel, L. Serrano, Structures in systems biology, Curr. Opin. Struct. Biol. 17 (2007) 378–384.
[4] M. Grabowski, A. Joachimiak, Z. Otwinowski, W. Minor, Structural genomics: keeping up with expanding knowledge of the protein universe, Curr. Opin. Struct. Biol. 17 (2007) 347–353.
[5] J. Weigelt, L.D. McBroom-Cerajewski, M. Schapira, Y. Zhao, C.H. Arrowmsmith, Structural genomics and drug discovery: all in the family, Curr. Opin. Chem. Biol. 12 (2008) 32–39.
[6] M.C. Smith, T.C. Furman, T.D. Ingolia, C. Pidgeon, Chelating peptide-immobilized metal ion affinity chromatography: a new concept in affinity chromatography for recombinant proteins, J. Biol. Chem. 263 (1988) 7211–7215.
[7] K. Terpe, Overview of tag protein fusions: from molecular and biochemical fundamentals to commercial systems, Appl. Microbiol. Biotechnol. 60 (2003) 523–533.

[8] D. Sachdev, J.M. Chirgwin, Fusions to maltose-binding protein: control of folding and solubility in protein purification, Methods Enzymol. 326 (2000) 312–321.
[9] D.B. Smith, Generating fusions to glutathione *S*-transferase for protein studies, Methods Enzymol. 326 (2000) 254–270.
[10] E.R. LaVallie, E.A. DiBlasio, S. Kovacic, K.L. Grant, P.F. Schendel, J.M. McCoy, A thioredoxin gene fusion expression system that circumvents inclusion body formation in the *E. coli* cytoplasm, Bio/Technology 11 (1993) 187–193.
[11] G.D. Davis, C. Elisee, D.M. Newham, R.G. Harrison, New fusion protein systems designed to give soluble expression in *Escherichia coli*, Biotechnol. Bioeng. 65 (1999) 382–388.
[12] R.B. Kapust, D.S. Waugh, *Escherichia coli* maltose-binding protein is uncommonly effective at promoting the solubility of polypeptides to which it is fused, Protein Sci. 8 (1999) 1668–1674.
[13] L. Niiranen, S. Espelid, C.R. Karlsen, M. Mustonen, S.M. Paulsen, P. Heikinheimo, N.P. Willassen, Comparative expression study to increase the solubility of cold adapted Vibrio proteins in *Escherichia coli*, Protein Expr. Purif. 52 (2007) 210–218.
[14] J.G. Marblestone, S.C. Edavettal, Y. Lim, P. Lim, X. Zuo, T.R. Butt, Comparison of SUMO fusion technology with traditional gene fusion systems: enhanced expression and solubility with SUMO, Protein Sci. 15 (2006) 182–189.
[15] S. Nallamsetty, D.S. Waugh, Solubility-enhancing protein MBP and NusA play a passive role in the folding of their fusion partners, Protein Expr. Purif. 45 (2006) 175–182.
[16] G.G. Privé, G.E. Verner, C. Weitzman, K.H. Zen, D. Eisenberg, H.R. Kaback, Fusion proteins as tools for crystallization: the lactose permease from *Escherichia coli*, Acta Crystallogr. D 50 (1994) 375–379.
[17] D.R. Smyth, M.K. Mrozkiewicz, W.J. Mcgrath, P. Listwan, B. Kobe, Crystal structures of fusion proteins with large-affinity tags, Protein Sci. 12 (2003) 1313–1322.
[18] J.P. Donahue, H. Patel, W.F. Anderson, J. Hawiger, Three-dimensional structure of the platelet integrin recognition segment of the fibrinogen gamma chain obtained by carrier protein-driven crystallization, Proc. Natl. Acad. Sci. USA 91 (1994) 12178–12182.
[19] B. Kobe, R.J. Center, B.E. Kemp, P. Poumbourios, Crystal structure of human T cell leukemia virus type 1 gp21 ectodomain crystallized as a maltose-binding protein chimera reveals structural evolution of retroviral transmembrane proteins, Proc. Natl. Acad. Sci. USA 96 (1999) 4319–4324.
[20] Y. Zhan, X. Song, G.W. Zhou, Structural analysis of regulatory protein domains using GST-fusion proteins, Gene 281 (2001) 1–9.
[21] E. Le Rouzic, N. Belaïdouni, E. Estrabaud, M. Morel, J.C. Rain, C. Transy, F. Margottin-Goguet, HIV-1 Vpr function is mediated by interaction with the damage specific DNA-binding protein DDB1, Cell Cycle 6 (2007) 182–188.
[22] B. Schrofelbauer, Y. Hakata, N.R. Landau, HIV-1 Vpr function is mediated by interaction with the damage specific DNA-binding protein DDB1, Proc. Natl. Acad. Sci. USA 104 (2007) 4130–4135.
[23] K. Hrecka, M. Gierszewska, S. Srivastava, L. Kozaczkiewicz, S.K. Swanson, L. Florensm, M.P. Washburn, J. Skowronski, Lentiviral Vpr usurps Cul4-DDB1[VprBP] E3 ubiquitin ligase to modulate cell cycle, Proc. Natl. Acad. Sci. USA 104 (2007) 11778–11783.
[24] X. Wen, K.M. Duus, T.D. Friedrich, C.M. de Noronha, The HIV-1 protein Vpr acts to promote G2 cell cycle arrest by engaging a DDB1 and Cullin4A-containing ubiquitin ligase complex using VprBP/DCAF1 as an adaptor, J. Biol. Chem. 282 (2007) 27046–27057.
[25] L. Tan, E. Ehrlich, X.F. Yu, DDB1 and Cul4A are required for human immunodeficiency virus type 1 Vpr-induced G2 arrest, J. Virol. 81 (2007) 10822–10830.
[26] E. Le Rouzic, S. Benichou, The Vpr protein from HIV-1: distinct roles along the viral life cycle, Retrovirology 2 (2005) 11.
[27] K. Miyauchi, J. Komano, Y. Yokomaku, W. Sugiura, N. Yamamoto, Z. Matsuda, Role of the specific amino acid sequence of the membrane-spanning domain of human immunodeficiency virus type 1 in membrane fusion, J. Virol. 79 (2005) 4720–4729.
[28] Structural-Biological Whole Cell Project. Available from: <http://www.thermus.org>.
[29] H. Iino, H. Naitow, Y. Nakamura, N. Nakagawa, Y. Agari, M. Kanagawa, A. Ebihara, A. Shikai, M. Sugahara, M. Miyano, N. Kamiya, S. Yokoyama, K. Hirotsu, S. Kuramitsu, Crystallization screening test for the Whole-Cell Project on *Thermus thermophilus* HB8, Acta Crystallogr. F 64 (2008) 487–491.
[30] T. Oshima, K. Imahori, Description of *Thermus thermophilus* (Yoshida and Oshima) comb. nov., a nonsporulating thermophilic bacterium from a Japanese thermal spa, Int. J. Syst. Bacteriol. 24 (1974) 102–112.
[31] S. Yokoyama, H. Hirota, T. Kigawa, T. Yabuki, M. Shirouzu, T. Terada, Y. Ito, Y. Matsuo, Y. Kuroda, Y. Nishimura, Y. Kyogoku, K. Miki, R. Masui, S. Kuramitsu, Structural genomics projects in Japan, Nat. Struct. Biol. 7 (2000) 943–945.
[32] RIKEN Bioresource Center DNA Bank, *Thermus thermophilus*. Available from: <http://www.brc.riken.jp/lab/dna/en/thermus_en.html>.
[33] S. Cabantous, T.C. Terwilliger, G.S. Waldo, Protein tagging and detection with engineered self-assembling fragments of green fluorescent protein, Nat. Biotechnol. 23 (2005) 102–107.
[34] P. Henklein, K. Bruns, M.P. Sherman, U. Tessmer, K. Licha, J. Kopp, C.M. de Noronha, W.C. Greene, V. Wray, U. Schubert, Functional and structural characterization of synthetic HIV-1 Vpr that transduces cells, localizes to the nucleus, and induces G2 cell cycle arrest, J. Biol. Chem. 275 (2000) 32016–32026.
[35] L. Slabinski, L. Jaroszewski, A.P. Rodrigues, L. Rychlewski, I.A. Wilson, S.A. Lesley, A. Godzik, The challenge of protein structure determination lessons from structural genomics, Protein Sci. 16 (2007) 247–282.
[36] A.H. Podmore, P.E. Reynolds, Purification and characterization of VanXYC, a D,D-dipeptidase/D,D-carboxypeptidase in vancomycin-resistant *Enterococcus gallinarum* BM4174, Eur. J. Biochem. 269 (2002) 2740–2746.
[37] M. Taniguchi, T. Yoshimi, K. Hongo, T. Mizobata, Y. Kawata, Stopped-flow fluorescence analysis of the conformational changes in the GroEL apical domain: relationships between movements in the apical domain and the quaternary structure of GroEL, J. Biol. Chem. 279 (2004) 16368–16376.
[38] M. Yokokawa, C. Wada, T. Ando, N. Sakai, A. Yagi, S.H. Yoshimura, K. Takeyasu, Fast-scanning atomic force microscopy reveals the ATP/ADP-dependent conformational changes of GroEL, EMBO J. 25 (2006) 4567–4576.
[39] K. Arora, C.L. Brooks III, Large-scale allosteric conformational transitions of adenylate kinase appear to involve a population-shift mechanism, Proc. Natl. Acad. Sci. USA 104 (2007) 18496–18501.
[40] P.C. Whitford, S. Gosavi, J.N. Onuchic, Conformational transitions in adenylate kinase: allosteric communication reduces misligation, J. Biol. Chem. 283 (2008) 2042–2048.
[41] A.L. Horwich, G.W. Farr, W.A. Fenton, GroEL-GroES-mediated protein folding, Chem. Rev. 106 (2006) 1917–1930.
[42] P. Goloubinoff, A.A. Gatenby, G.H. Lorimer, GroE heat-shock proteins promote assembly of foreign prokaryotic ribulose bisphosphate carboxylase oligomers in *Escherichia coli*, Nature 337 (1989) 44–47.
[43] S.C. Lee, P.O. Olins, Effect of overproduction of heat shock chaperones GroESL and DnaK on human procollagenase production in *Escherichia coli*, J. Biol. Chem. 267 (1992) 2849–2852.
[44] P. Caspers, M. Stieger, P. Burn, Overproduction of bacterial chaperones improves the solubility of recombinant protein tyrosine kinases in *Escherichia coli*, Cell. Mol. Biol. 40 (1994) 635–644.
[45] K.E. Amrein, B. Takacs, M. Stieger, J. Molnos, N.A. Flint, P. Burn, Purification and characterization of recombinant human p50csk protein–tyrosine kinase from an *Escherichia coli* expression system overproducing the bacterial chaperones GroES and GroEL, Proc. Natl. Acad. Sci. USA 92 (1995) 1048–1052.
[46] K. Nishihara, M. Kanemori, H. Yanagi, T. Yura, Overexpression of trigger factor prevents aggregation of recombinant proteins in *Escherichia coli*, Appl. Environ. Microbiol. 66 (2000) 884–889.
[47] K. Amada, M. Yohda, M. Odaka, I. Endo, N. Ishii, H. Taguchi, M. Yoshida, Molecular cloning, expression, and characterization of chaperonin-60 and chaperonin-10 from a thermophilic bacterium, *Thermus thermophilus* HB8, J. Biochem. 118 (1995) 347–354.

ELSEVIER

INSTITUT PASTEUR

Microbes and Infection 11 (2009) 191–197

www.elsevier.com/locate/micinf

Original article

Activation of HIV-1 Gag-specific CD8$^+$ T cells by yeast-derived VLP-pulsed dendritic cells is influenced by the level of mannose on the VLP antigen

Fuminori Mizukoshi [a], Takuya Yamamoto [a], Yu-ya Mitsuki [a], Kazutaka Terahara [a], Ai Kawana-Tachikawa [b], Kazuo Kobayashi [a], Aikichi Iwamoto [b], Yuko Morikawa [c], Yasuko Tsunetsugu-Yokota [a,*]

[a] *Department of Immunology, National Institute of Infectious Diseases, Toyama 1-23-1 Shinjuku-ku, Tokyo, Japan*
[b] *Department of Infectious Diseases, Institute of Medical Science, University of Tokyo, Shirokanedai 4-6-1, Minato-ku, Tokyo, Japan*
[c] *Kitasato Institute for Life Sciences and Graduate School for Infection Control, Kitasato University, Shirokane 5-9-1, Minato-ku, Tokyo, Japan*

Received 3 October 2008; accepted 12 November 2008
Available online 24 November 2008

Abstract

Dendritic cells (DCs) are professional antigen-presenting cells that possess a unique capacity to cross-present exogenous antigens efficiently to CD8$^+$ T cells. We previously demonstrated that monocyte-derived DCs (MDDCs) pulsed with yeast-derived HIV-1 Gag virus-like particles (VLPs) were able to activate Gag-specific CD8$^+$ T cells from HIV-1-infected individuals. Yeast VLPs are abundantly mannosylated (high-mannose type: HmVLPs) and are highly immunogenic. Because lectin receptors are shown to negatively regulate Th1 responses, we investigated the relationship between VLP mannosylation level and MDDC cross-presentation activity. Poorly mannosylated VLPs (low-mannose type: LmVLPs) were prepared using a yeast mnn9 mutant strain that lacks a core mannosylation enzyme. We found that MDDCs pulsed with LmVLPs activated Gag-specific T cells more strongly than those pulsed with HmVLPs. However, MDDCs showed similar antigen uptake and intracellular transport of both types of VLPs. Interestingly, LmVLPs induced IL-12 production slightly more than HmVLPs (yet statistically significant). Furthermore, the level of LPS-induced IL-10 production was enhanced by pulsing with HmVLPs, but not with LmVLPs. These results indicate that lectin receptors recognizing mannose may influence the Th1/Th2 balance of the immune response, resulting in reduced efficiency of CD8$^+$ T cell activation by a heavily mannosylated antigen presented by DCs.

Keywords: Antigen presentation; Mannosylation; AIDS

1. Introduction

Dendritic cells (DCs) are professional antigen-presenting cells that play a pivotal role in the immune system by acting as "sentinel cells" [1]. DC-based immunotherapy has been developed to treat a variety of diseases, including cancer [2,3], autoimmune diseases [4], transplant rejection [5], allergic diseases [6], and infectious diseases [7]. Previous studies of human immunodeficiency virus (HIV) and simian immunodeficiency virus (SIV) infections demonstrated that monocyte-derived DCs (MDDCs) pulsed with inactivated viruses enhanced both cellular and humoral immune responses [8,9]. However, the efficacies of DC-based immunotherapy for clinical applications have been inconsistent, probably because of the different protocols for cultivating and maturating the DCs, for the selection and loading of antigens, and for the administration, route, dose, and frequency of the therapy.

* Corresponding author: Tel.: +81 3 5285 1111x2133; fax: +81 3 5285 1150 or 1156.
E-mail address: yyokota@nih.go.jp (Y. Tsunetsugu-Yokota).

1286-4579/$ - see front matter Crown Copyright © 2008 Published by Elsevier Masson SAS. All rights reserved.
doi:10.1016/j.micinf.2008.11.004

Acquired immune deficiency syndrome (AIDS), which is caused by HIV infection, is an enormous public health threat worldwide. The development of highly active anti-retroviral therapy (HAART) has markedly improved treatment of HIV-infected individuals and has significantly reduced HIV-associated mortality [10]. However, HAART cannot completely eradicate HIV [11]. Therefore, a novel strategy is required for treating HIV infections.

In terms of the host immune response against HIV, antigen-specific $CD8^+$ cytotoxic T lymphocytes (CTLs) are known to be important in suppressing HIV replication [12]. Therefore, CTL-inducible vaccines have been developed, most of them virus-based [13]. We previously showed that DCs pulsed with yeast-derived HIV-1 Gag virus-like particles (VLPs) activated Gag-specific T cells *in vitro* [14]. Because VLPs are neither infectious nor replicative, and also can be easily produced on a large scale, a VLP-based vaccine is an excellent candidate for a vaccine based on cross-presentation.

Highly glycosylated antigens have strong immunogenicity, whether expressed by yeast or using a baculoviral system. For example, mannosylation of antigens augments antigen-specific T cell responses [15,16]. However, recent studies revealed that the stimulation of lectin receptors on DCs induced interleukin (IL)-10 production, resulting in a shift in immune regulation towards Th2 dominance [17–19]. Thus, the influence of carbohydrate chains on the immune response is a concern for novel vaccine developments.

We postulated that the cross-presentation activity of DC is influenced by the degree of antigen mannosylation. In this study, we compared the antigenicity of abundantly mannosylated VLPs derived from a wild-type yeast to that of poorly mannosylated VLPs derived from a yeast mnn9 mutant lacking mannosylating enzyme.

2. Materials and methods

2.1. Preparation of cells

Fresh peripheral blood mononuclear cells (PBMCs) were obtained from healthy donors by Ficoll density gradient centrifugation. $CD14^+$ cells were positively isolated from PBMCs using a MACS system (Miltenyi Biotech, Bergisch Gladbach, Germany) according to the manufacturer's protocol. We generated immature MDDCs using 10 ng/ml human granulocyte-macrophage colony-stimulating factor and 20 ng/ml IL-4 as previously described [14]. These blood samples were collected with written informed consent under the approval of the ethical committee in National Institute of Infectious Diseases (NIID).

A Gag28 peptide (p17:KYKLKHIVW)-specific CTL line was established from PBMCs of HIV-1-infected individuals carrying HLA-A*2402 as previously described [20]. The studies utilizing PBMCs of HIV-infected patients were approved by the ethical committees in NIID and the Institute of Medical Science (University of Tokyo), and PBMCs were collected with written informed consent.

2.2. Production and purification of yeast-derived HIV-1 Gag VLPs

Wild-type yeast-derived VLPs from HIV-1 Gag, VLPs fused with green fluorescent protein (EGFP) and control culture supernatant (CS) were produced as described previously [14,21]. The mutant *S. cerevisiae* mnn9 strain [22] was used to produce low mannose-type VLPs. Standard purification and sucrose density gradient analysis of Gag VLPs was performed as described previously [23]. Purified VLPs were obtained by fractionation of the gradients. For comparison, *Spodoptera frugiperda* (*Sf9*) cells were infected with recombinant *Autographa californica* nuclear polyhedrosis viruses (baculoviruses) containing the full-length HIV-1 *gag* gene [23]. Purified Gag VLPs were quantitated by Coomassie brilliant blue staining. Total yeast protein was quantified by Bradford's method [21].

2.3. Quantitative analysis of mannose on the VLPs with dot blot technique

The samples were diluted with PBS and applied to a nitrocellulose membrane (0.45 μm pore size; GE Osmonics Labstore, Minnetonka, MA) using BioDot SF microfiltration apparatus (BioRad, Hercules, CA) according to the manufacturer's instructions. The membrane was soaked three times in blocking buffer (10 mM Tris–HCl pH 7.4, 0.15 M NaCl, 0.05% Tween20) for 10 min at room temperature (RT), then reacted with the biotinylated ConA (EY Laboratories, Inc., San Mateo, CA) (10 μg/ml in blocking buffer) for 90 min. After washing three times with blocking buffer, the membrane was incubated for 30 min at RT with horseradish peroxidase (HRP)-conjugated streptavidin (Boehringer-Roche, Basel, Switzerland) (1:5000 dilution). The SuperSignal West Dura kit (Pierce, Rockford, IL) was used for detection and the signal was analyzed by LAS-3000 (Fujifilm, Tokyo, Japan). The luminescence intensity of each dot was measured using Image Gauge densitometry software (version 4.0; Fujifilm).

2.4. Endocytosis assay

Immature MDDCs were incubated with various concentrations of CS or high- or low-mannose type VLP-EGFP at 37 °C for 3 h. These cells were washed extensively with flow cytometry (FCM) buffer (2% v/v fetal bovine serum and 50 μg/ml sodium azide in PBS), and resuspended in FCM buffer containing propidium iodide. The uptake of VLP-EGFP was quantified by measuring the fluorescence intensity using FACScalibur and CellQuest software (Becton Dickinson, Labware, NJ). For the receptor blocking assay, immature MDDCs were pre-cultured for 30 min in the presence of mAb against dendritic cell-specific intracellular adhesion molecule-3-grabbing nonintegrin (DC-SIGN) (10 μg/ml; eBioscience, San Diego, CA), mannose receptor (MR) mAb (10 μg/ml; BD Bioscience, Flanklin Lakes, NJ), mannan (2 mg/ml; Sigma–Aldrich) or isotype control IgG_{2a} (10 μg/ml; eBioscience), then pulsed with VLPs (10 μg/ml) or fluorescein-isothiocyanate

(FITC)-conjugated mannosylated BSA (man-BSA; Sigma–Aldrich) (100 μg/ml).

2.5. Subcellular fractionation and Western blotting analysis

Immature MDDCs cultured with 40 μg/ml of high- or low-mannose type VLPs were washed with PBS and then fractionated into cytosol and membrane/organelle fractions using ProteoExtract subcellular proteome extraction kit (Calbiochem, Darmstadt, Germany).

For Western blotting, cells or subcellular fractions were resuspended in lysis buffer (10 mM Tris–HCl pH 7.4, 150 mM NaCl, 1% sodium deoxycholate, 1% Triton X-100, 0.1% sodium dodecyl sulfate, 357.5 mM 2-mercaptoethanol). The lysate, containing 2×10^5 cells, was analyzed by 12.5% SDS-PAGE and electrophoretically transferred to a PVDF transfer membrane (Amersham Biosciences, Buckinghamshire, UK). Non-specific binding was blocked with washing buffer (10 mM Tris–HCl, 150 mM NaCl, 0.05% Tween 20) containing 3% skim milk for 30 min at RT. After washing, the membrane was stained for 1 h at RT either with the anti-Calpain mAb (Calbiochem) as a cytosolic marker or anti-gastrin-releasing peptide (GRP) 78 mAb (BD Bioscience) as a membrane/organelle marker. Subsequently, the membrane was incubated with biotin-conjugated anti-mouse IgG for 1 h at RT, followed by streptavidin-conjugated HRP (Boehringer-Roche) for 30 min at RT. Gag p24 was detected by incubation with HRP-conjugated anti-HIV Gag mAbs (clone 10B5; kindly provided by T. Sata, Department of Pathology, NIID, Tokyo, Japan) [24] for 1 h at RT. The immunoreactive bands were detected with SuperSignal West Dura kit and visualized by Lumino analyzer LAS-3000.

2.6. Detection of cytokines

To detect IFN-γ production, an enzyme-linked immunospot (ELISPOT) assay was carried out as previously described [14]. The culture supernatant was collected and the level of cytokines was measured with the cytometric beads array kit (BD Bioscience) according to the manufacturer's protocol.

3. Results

3.1. Characterization of VLPs generated from yeast mutant mnn9

To determine whether the level of antigen mannosylation can modulate the immune response, we generated VLPs from wild-type yeast and from the mannosyltransferase mutant mnn9. The mnn mutants are mostly defective in polymerization enzymes related to the synthesis of the outer chain portion of N-linked oligosaccharides, and the mnn9 strain is defective in the core enzyme for glycosylation [25]. The wild-type yeast-derived VLPs are heavily mannosylated and are designated as high-mannose type VLPs (HmVLPs); in contrast, mnn9 mutants produce poorly mannosylated VLPs (low-mannose type VLPs: LmVLPs). The mannosylation level of LmVLPs is considered to be more similar to the level of mannose on mammalian mannoproteins than that of HmVLPs.

Using sucrose density gradient analysis, HmVLPs were recovered mainly at the density of 1.210 g/ml (Fig. 1A, upper panel), while the major peak density of LmVLPs was at 1.196 g/ml (Fig. 1A, middle panel) and the major peak of baculovirus-based VLPs was at 1.180 g/ml (Fig. 1A, lower panel). Thus, the LmVLPs are smaller in size than HmVLPs, probably due to the lower degree of mannosylation.

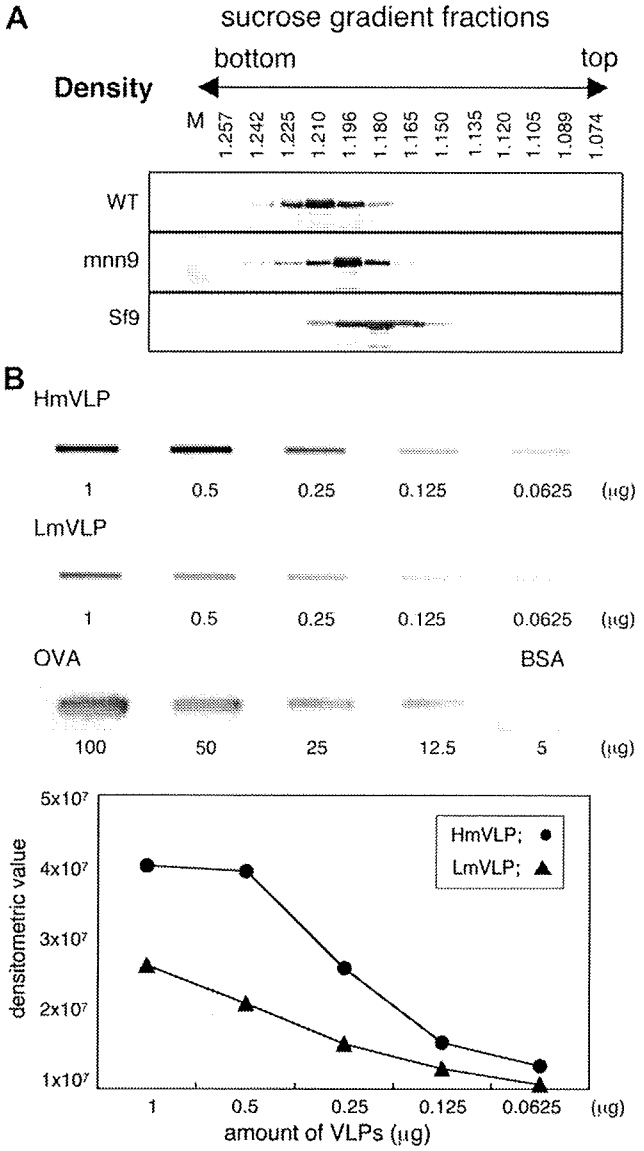

Fig. 1. Characterization of yeast VLPs. (A) Sucrose density gradient fractions were analyzed by Western blotting using anti-Gag mAbs. (Upper panel) HmVLPs derived from wild-type *S. cerevisiae* (WT). (Middle panel) LmVLPs derived from mnn9 mutant strain (mnn9). (Lower panel) VLPs derived from Sf9. 40 μg of VLPs were applied per assay, respectively. (B) Lectin staining was carried out on using biotinylated ConA and HRP-conjugated avidin. The number is indicative of the volume of sample applied per slot. The densitometric value of HmVLPs (filled circle) or LmVLPs (filled triangle) was measured by the computerization.

We next estimated the level of the mannosylation on these VLPs using lectin blot. In comparison with the LmVLPs generated from the mnn9 mutants, HmVLPs generated from a wild-type yeast strain clearly showed higher levels of mannose (Fig. 1B). As control, no mannose was detected in native BSA, while OVA was highly mannosylated. These results indicate that LmVLPs and HmVLPs differ in their mannose glycosylation levels.

3.2. The effect of uptake and intracellular dynamics of HmVLPs and LmVLPs

We first studied the internalization efficiency of EGFP-fused VLPs by MDDCs. We titrated the uptake of these VLPs at various concentrations (5–20 μg/ml). Both VLPs were taken up by MDDCs in a dose-dependent manner (Fig. 2A, upper panels), although the uptake of HmVLP was slightly better than that of LmVLP at 5 μg/ml.

In order to understand the mechanism of uptake of these VLPs by MDDCs, we carried out the blocking experiment. The uptake of these HmVLP and LmVLP at 10 μg/ml was strongly inhibited by mannan, but neither by anti-MR nor by anti-DC-SIGN mAbs (Fig. 2A, lowest panels). In contrast, the uptake of a high dose of man-BSA was remarkably inhibited by the same concentration of anti-MR, but not by anti-DC-SIGN mAb. Therefore, MDDCs are able to take up these VLPs at a similar level, probably by the mannose-mediated mechanism, but neither via DC-SIGN nor MR.

For cross-presentation of VLPs, the antigens incorporated in MDDCs have to be transported into the cytosol and processed by the proteasomes. To test whether the intracellular transport of VLPs is influenced by their level of mannosylation, the MDDCs were pulsed for 1 or 6 h with the

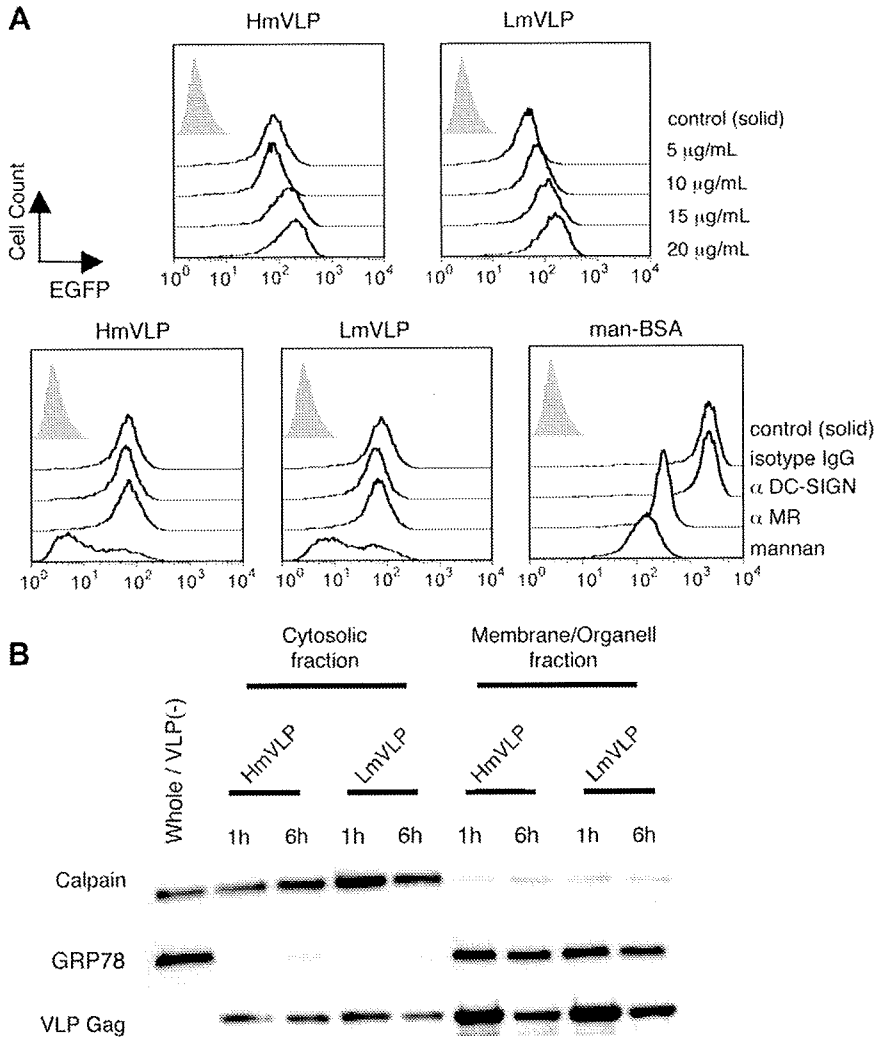

Fig. 2. Uptake and localization of yeast VLPs by DCs. (A) Immature MDDCs (5×10^4 cells/50 μl) were incubated with HmVLP-EGFP or LmVLP-EGFP (upper panel, indicated concentrations; lower panel, 10 μg/ml) for 3 h, analyzed by flow cytometry. Moreover, MDDCs were pre-incubated for 30 min with indicated antibodies (10 μg/ml) or mannan (2 mg/ml), and pulsed with HmVLP-EGFP or LmVLP-EGFP (10 μg/ml), mannosylated BSA (100 μg/ml) as a control (lower panel). The background signal is shown as a shadow. (B) Immature MDDCs (1×10^6 cells/200 μl) were incubated with 40 μg/ml yeast HmVLPs, LmVLPs or CS for 1 or 6 h, and fractionated. Whole cell lysate [Whole/VLP(−)] and cytosolic and membrane/organelle fractions were analyzed by Western blotting using antibodies against the cytosolic marker Calpain, the membrane marker GFP78, and VLP Gag.

VLPs at a high concentration (40 μg/ml) to obtain a strong signal, and fractionated. The level of HIV-1 Gag protein in the cytosolic and membrane/organelle fractions was analyzed by Western blot (Fig. 2B). As control, the calpain was detected mainly on the cytosolic fraction, whereas GRP78 was detected exclusively on the membrane/organelle fraction. There was no clear difference in the amount of Gag protein present in the cytosolic fractions in MDDCs pulsed with HmVLPs versus LmVLPs, as well as in the membrane/organelle fraction. We concluded that the mannosylation level of VLPs does not affect the internalization or the intracellular amount of Gag antigens in MDDCs.

3.3. LmVLPs are more efficiently cross-presented than HmVLPs for CD8$^+$ T cell (CTLs) activation by MDDCs

We next tested the efficiency of these VLPs on CTL activation by MDDC-mediated cross-presentation. We utilized HIV-1 Gag28 peptide-specific CTL lines established from HLA-A24$^+$ HIV-infected patients as an indicator cell for cross-presentation efficiency. Frozen HLA-A24$^+$ healthy donor-derived MDDCs were pulsed either with 10 μg/ml of HmVLPs or LmVLPs, cocultured with Gag-specific CTL lines for 40 h, and analyzed by IFN-γ ELISPOT.

For this experiment, three independent CTL lines (CTL #9, #21, and #31) were cocultured with VLP-pulsed MDDCs derived from two donors each (Fig. 3). Despite the MDDCs' donor variation, LmVLP-pulsed MDDCs were able to activate higher numbers of Gag28-specific CTL lines compared to HmVLP-pulsed MDDCs in four of six MDDCs. Thus, our results suggest that the level of mannose on antigens can modulate the cross-presenting activity of VLPs by MDDCs.

3.4. Cytokine production by MDDCs after uptake of VLPs is influenced by the level of VLP mannosylation

For effective induction of CTL activity, it is important to polarize DCs toward Th1-type cytokine secretion during the DC–T cell interaction. We previously showed that MDDCs stimulated with yeast VLPs produced a higher level of IL-12 than those stimulated with LPS, while IL-10 production is limited [14]. We therefore measured cytokine production by 10 μg/ml of HmVLP- or LmVLP-pulsed MDDCs from eight healthy donors. Two patterns of IL-12 production were identified: IL-12 responders ($n = 4$), and IL-12 non-responders ($n = 4$) (Fig. 4).

In the case of the IL-12 responders, IL-12 production induced by LmVLPs tended to be higher than that by HmVLP (Fig. 4A), though the difference was not statistically significant. In contrast, the level of IL-10 production was very low in these donors (data not shown).

In IL-12 non-responders, both IL-12 and IL-10 production by LmVLP- or HmVLP-pulsed MDDCs were consistently low (data not shown). When we stimulated the MDDCs from these donors with LPS, the production of IL-10, but not IL-12, was increased, and the LPS-induced IL-10 production

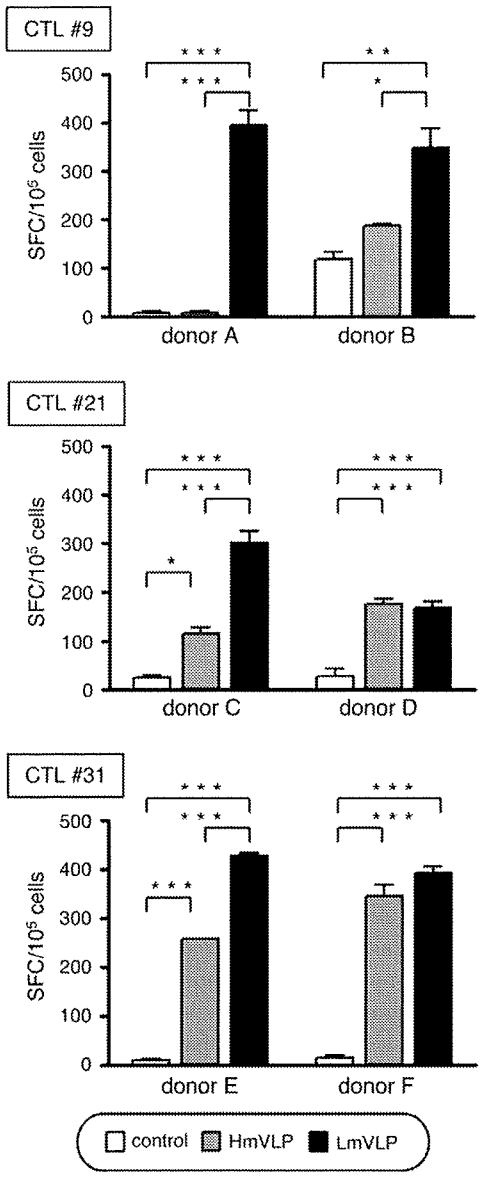

Fig. 3. The influence of yeast VLPs on HIV Gag-specific CD8$^+$ T cell activation. Immature MDDCs were pulsed overnight with 10 μg/ml HmVLPs (gray bar), LmVLPs (filled bar), or CS (open bar). Next day, MDDCs (1×10^4 cells per well) were mixed with MHC class I-matched allogenic CTL clones ($1–2 \times 10^4$ per well). Two days after cocultivation, the number of IFN-γ-producing cells was determined by ELISPOT analysis. The longitudinal axis shows the analysis spot forming cells (SFC) producing IFN-γ per 10^5 cells. Results are presented as the means + SEM. $^*P < 0.05$; $^{**}P < 0.01$; $^{***}P < 0.001$, compared between two groups; one-way ANOVA followed by Bonferroni's *t*-test ($n = 3$).

was upregulated further in the presence of HmVLPs, while it was not true for LmVLPs (Fig. 4B). The level of IL-12 production remained undetectable or low even after stimulation with LPS plus HmVLPs or LPS plus LmVLPs (data not shown). The production of other cytokines (including IL-1, IL-6, IL-8, and TNF-alpha) was very low or showed little difference in response to HmVLPs and LmVLPs. These results suggest that a high level of mannosylation modulates the cytokine production by MDDCs toward a Th2-type response.

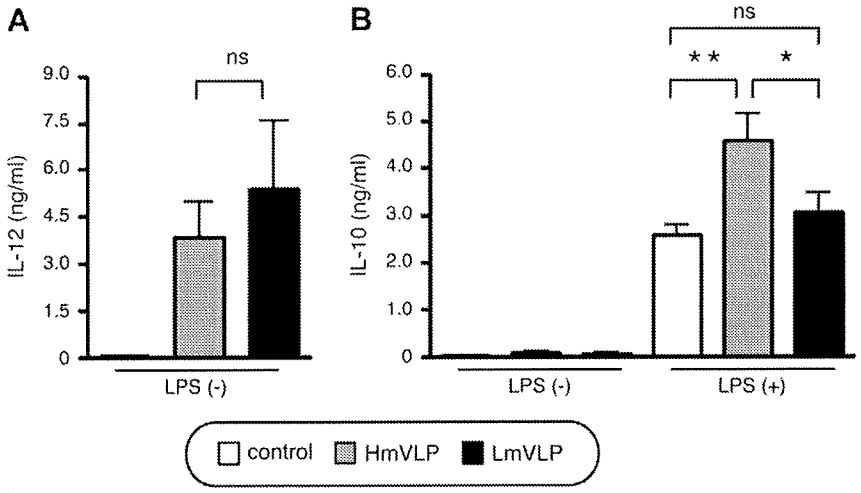

Fig. 4. The effect of yeast VLPs on cytokine production. (A) In the cases of IL-12 responders ($n = 4$), immature MDDCs (2×10^5 cells/200 μl) were incubated with 20 μg/ml HmVLPs (gray bar), LmVLPs (filled bar), or CS (open bar) for 24 h. (B) The MDDCs (2×10^5 cells/200 μl) of IL-12 non-responders ($n = 4$) were incubated with 20 μg/ml HmVLPs (gray bar), LmVLPs (filled bar), or CS (open bar) with or without 100 ng/ml LPS for 24 h. The cytokines produced by these cells were analyzed. Results are presented as the means + SEM. $^*P < 0.05$; $^{**}P < 0.01$; ns, not significant, compared between two groups; one-way ANOVA followed by Bonferroni's t-test ($n = 4$, respectively).

4. Discussion

Antigens expressed by yeast and insect cells contain abundant carbohydrate modifications and are perceived to be excellent vaccine antigens. Consistent with these observations, we previously demonstrated that MDDCs loaded with yeast-derived HIV-1 $p55^{gag}$ VLPs activated Gag-specific $CD8^+$ T cells in chronically-infected HIV patients [14]. Mannosylated antigens taken up by DCs are more efficiently presented to T cells than antigens internalized via fluid phase [15]. However, recent studies have indicated that excessive mannosylation leads to a Th2-dominant response or even suppresses the immune response via a signal from the lectin receptors [17–19]. Therefore, it is important to determine whether the level of mannosylation on VLPs positively or negatively affects the DC-based immune response.

The cell wall of *Saccharomyces cerevisae* is rich in mannoproteins. In this work, we used a yeast mnn9 mutant of the mannosyltransferase, which cannot synthesize completely glycosylated mannoproteins, and demonstrated that VLPs with much reduced mannose induced stronger CTL activation than more heavily mannosylated VLPs derived from wild-type yeast did. Because we used the same amount of Gag protein composed of these VLPs, the difference should be only at the level of glycosylation on VLPs. The efficiency of CTL activation by VLP-pulsed MDDCs was analyzed at 10–20 μg/ml concentration of VLPs. At this concentration, we detected no difference of uptake by FACS analysis. We speculate that the difference, if any, may be not at the level of uptake, but rather during antigen processing or loading to MHC class I. Although we failed to show the difference in the intracellular fate of these VLPs by the current technology, it is still possible that they are differently processed somewhere in the cytoplasm. In this context, it has been demonstrated previously that only a small amount (200 molecules) of peptide and MHC class I complex is enough to be recognized by CTLs [26]. Therefore, even a small difference in the antigen processing process may affect the efficiency of cross-presentation by DCs.

The balance of the Th1/Th2 immune response is influenced by elements such as host conditions and the antigen formulation [27]. LmVLPs induced IL-12 production slightly better than HmVLPs in some donors, whereas in those who do not produce a substantial level of IL-12, LPS-induced IL-10 production was increased by adding HmVLPs, but not by LmVLPs. A number of studies have demonstrated that cytokine production can be altered by the interaction of antigen with lectin receptors and/or toll-like receptors [17–19,28]. For example, Nigou et al. reported that the IL-12 production of DCs induced by LPS was negatively regulated by the engagement of an MR using mannose-capped lipoarabinomannans (the ManLAMs) of *Mycobacteria* [28]. Gringhuis et al. reported that stimulation of DC-SIGN by pathogens such as *Mycobacteria*, fungi, and viruses enhanced toll-like receptor signaling via Raf-1 kinase-dependent acetylation of the transcription factor NF-kB, resulting in strong augmentation of IL-10 mRNA expression by DCs [19]. Thus, stimulation of lectin receptors may preferentially induce IL-10 production in low IL-12 responders. We speculate that a mannosylation-dependent signal affects the Th1/Th2 balance by modulating the cytokine production of DCs, leading to the alternation of CTL activation.

In conclusion, a high level of mannosylation on an antigen may not necessarily be beneficial for CTL induction by DCs. The quantity of carbohydrate chain may alter the Th1/Th2 cytokine balance. DC-based immune therapy that aims to induce CTLs requires optimizing the antigen for the most effective clinical results. Further studies are required to develop the technology for modulating the antigenic property so that it can efficiently induce Th-1 type immune response.

One possible technology may be the modification of the outer structure, amount and variation of sugars moieties on vaccine antigens.

Acknowledgments

We are grateful to T. Sata (Department of Pathology, NIID, Tokyo, Japan) for anti-HIV Gag mAbs (clone 10B5). We are indebted to T. Murakami (AIDS Research Center, NIID, Tokyo, Japan) for excellent technical advice on the subcellular fractionation experiment. This work was supported by a grant from the Ministry of Health, Labour, and Welfare of Japan. F. Mizukoshi receives support from the Japanese Foundation for AIDS Prevention.

References

[1] J. Banchereau, R.M. Steinman, Dendritic cells and the control of immunity, Nature 392 (1998) 245–252.
[2] J. Banchereau, A.K. Palucka, Dendritic cells as therapeutic vaccines against cancer, Nat. Rev. Immunol. 5 (2005) 296–306.
[3] C.G. Figdor, I.J. de Vries, W.J. Lesterhuis, C.J. Melief, Dendritic cell immunotherapy: mapping the way, Nat. Med. 10 (2004) 475–480.
[4] A.G. Thompson, R. Thomas, Induction of immune tolerance by dendritic cells: implications for preventative and therapeutic immunotherapy of autoimmune disease, Immunol. Cell Biol. 80 (2002) 509–519.
[5] T.E. Ichim, R. Zhong, W.P. Min, Prevention of allograft rejection by in vitro generated tolerogenic dendritic cells, Transpl. Immunol. 11 (2003) 295–306.
[6] H. Matsue, M. Kusuhara, K. Matsue, A. Takashima, Dendritic cell-based immunoregulatory strategies, Int. Arch. Allergy Immunol. 127 (2002) 251–258.
[7] J. Colino, C.M. Snapper, Dendritic cells, new tools for vaccination, Microbes Infect 5 (2003) 311–319.
[8] W. Lu, L.C. Arraes, W.T. Ferreira, J.M. Andrieu, Therapeutic dendritic-cell vaccine for chronic HIV-1 infection, Nat. Med. 10 (2004) 1359–1365.
[9] W. Lu, X. Wu, Y. Lu, W. Guo, J.M. Andrieu, Therapeutic dendritic-cell vaccine for simian AIDS, Nat. Med. 9 (2003) 27–32.
[10] R.J. Pomerantz, D.L. Horn, Twenty years of therapy for HIV-1 infection, Nat. Med. 9 (2003) 867–873.
[11] D. Finzi, J. Blankson, J.D. Siliciano, J.B. Margolick, K. Chadwick, T. Pierson, K. Smith, J. Lisziewicz, F. Lori, C. Flexner, T.C. Quinn, R.E. Chaisson, E. Rosenberg, B. Walker, S. Gange, J. Gallant, R.F. Siliciano, Latent infection of CD4+ T cells provides a mechanism for lifelong persistence of HIV-1, even in patients on effective combination therapy, Nat. Med. 5 (1999) 512–517.
[12] B.D. Walker, B.T. Korber, Immune control of HIV: the obstacles of HLA and viral diversity, Nat. Immunol. 2 (2001) 473–475.
[13] A. Duerr, J.N. Wasserheit, L. Corey, HIV vaccines: new frontiers in vaccine development, Clin. Infect. Dis. 43 (2006) 500–511.
[14] Y. Tsunetsugu-Yokota, Y. Morikawa, M. Isogai, A. Kawana-Tachikawa, T. Odawara, T. Nakamura, F. Grassi, B. Autran, A. Iwamoto, Yeast-derived human immunodeficiency virus type 1 p55(gag) virus-like particles activate dendritic cells (DCs) and induce perforin expression in Gag-specific CD8(+) T cells by cross-presentation of DCs, J. Virol. 77 (2003) 10250–10259.
[15] A.J. Engering, M. Cella, D. Fluitsma, M. Brockhaus, E.C. Hoefsmit, A. Lanzavecchia, J. Pieters, The mannose receptor functions as a high capacity and broad specificity antigen receptor in human dendritic cells, Eur. J. Immunol. 27 (1997) 2417–2425.
[16] M.C. Tan, A.M. Mommaas, J.W. Drijfhout, R. Jordens, J.J. Onderwater, D. Verwoerd, A.A. Mulder, A.N. van der Heiden, D. Scheidegger, L.C. Oomen, T.H. Ottenhoff, A. Tulp, J.J. Neefjes, F. Koning, Mannose receptor-mediated uptake of antigens strongly enhances HLA class II-restricted antigen presentation by cultured dendritic cells, Eur. J. Immunol. 27 (1997) 2426–2435.
[17] E. Caparros, P. Munoz, E. Sierra-Filardi, D. Serrano-Gomez, A. Puig-Kroger, J.L. Rodriguez-Fernandez, M. Mellado, J. Sancho, M. Zubiaur, A.L. Corbi, DC-SIGN ligation on dendritic cells results in ERK and PI3K activation and modulates cytokine production, Blood 107 (2006) 3950–3958.
[18] T.B. Geijtenbeek, S.J. Van Vliet, E.A. Koppel, M. Sanchez-Hernandez, C.M. Vandenbroucke-Grauls, B. Appelmelk, Y. Van Kooyk, *Mycobacteria* target DC-SIGN to suppress dendritic cell function, J. Exp. Med. 197 (2003) 7–17.
[19] S.I. Gringhuis, J. den Dunnen, M. Litjens, B. van Het Hof, Y. van Kooyk, T.B. Geijtenbeek, C-type lectin DC-SIGN modulates Toll-like receptor signaling via Raf-1 kinase-dependent acetylation of transcription factor NF-kappaB, Immunity 26 (2007) 605–616.
[20] A. Kawana-Tachikawa, M. Tomizawa, J. Nunoya, T. Shioda, A. Kato, E.E. Nakayama, T. Nakamura, Y. Nagai, A. Iwamoto, An efficient and versatile mammalian viral vector system for major histocompatibility complex class I/peptide complexes, J. Virol. 76 (2002) 11982–11988.
[21] S. Sakuragi, T. Goto, K. Sano, Y. Morikawa, HIV type 1 Gag virus-like particle budding from spheroplasts of Saccharomyces cerevisiae, Proc. Natl. Acad. Sci. USA 99 (2002) 7956–7961.
[22] C.E. Ballou, Isolation, characterization, and properties of *Saccharomyces cerevisiae* mnn mutants with nonconditional protein glycosylation defects, Methods Enzymol 185 (1990) 440–470.
[23] Y. Morikawa, S. Hinata, H. Tomoda, T. Goto, M. Nakai, C. Aizawa, H. Tanaka, S. Omura, Complete inhibition of human immunodeficiency virus Gag myristoylation is necessary for inhibition of particle budding, J. Biol. Chem. 271 (1996) 2868–2873.
[24] Y. Tsunetsugu-Yokota, K. Akagawa, H. Kimoto, K. Suzuki, M. Iwasaki, S. Yasuda, G. Hausser, C. Hultgren, A. Meyerhans, T. Takemori, Monocyte-derived cultured dendritic cells are susceptible to human immunodeficiency virus infection and transmit virus to resting T cells in the process of nominal antigen presentation, J. Virol. 69 (1995) 4544–4547.
[25] C.E. Ballou, Yeast cell wall and cell surface, in: J.N. Stranthern, E.W. Jones, J.R. Broach (Eds.), The Molecular Biology of the Yeast Saccharomyces, Metabolism and Gene Expression, Cold Spring Harbor Laboratory Press, Cold Spring Harbor, NY, 1982, pp. 335–360.
[26] E.R. Christinck, M.A. Luscher, B.H. Barber, D.B. Williams, Peptide binding to class I MHC on living cells and quantitation of complexes required for CTL lysis, Nature 352 (1991) 67–70.
[27] P. Kidd, Th1/Th2 balance: the hypothesis, its limitations, and implications for health and disease, Altern. Med. Rev. 8 (2003) 223–246.
[28] J. Nigou, C. Zelle-Rieser, M. Gilleron, M. Thurnher, G. Puzo, Mannosylated lipoarabinomannans inhibit IL-12 production by human dendritic cells: evidence for a negative signal delivered through the mannose receptor, J. Immunol. 166 (2001) 7477–7485.

Highly restricted T-cell receptor repertoire in the CD8$^+$ T-cell response against an HIV-1 epitope with a stereotypic amino acid substitution

Eriko Miyazaki[a,*], Ai Kawana-Tachikawa[a,*], Mariko Tomizawa[a], Jun-ichi Nunoya[a], Takashi Odawara[a], Takeshi Fujii[b], Yi Shi[d], George Fu Gao[d] and Aikichi Iwamoto[a,b,c]

Objective: In peripheral blood mononuclear cells (PBMCs) from HIV-1-positive patients, we sought to identify CD8$^+$ T-cell populations and the corresponding T-cell receptor (TCR) repertoires that react to an immunogenic cytotoxic T lymphocyte (CTL) epitope with or without an escape mutation.

Methods: PBMCs from HLA-A*2402(A24)-positive patients were stimulated with peptides representing a wild-type CTL epitope in the HIV-1 Nef protein [Nef138-10(wt)] or an escape mutant with a Y to F (Y139F) substitution at the second position [Nef138-10(2F)]. Cultured PBMCs were stained with peptide-major histocompatibility complex tetramers containing Nef138-10(wt) or Nef138-10(2F) sequences. After in-vitro stimulation of PBMCs with cognate peptides, the CD8$^+$ T-cell population was sorted into different fractions: positive only to the wild-type tetramer (wt-positive), positive only to the mutant tetramer (2F-positive), and positive to both wt-tetramers and mutant-tetramers (dual-positive). TCR repertoires of sorted epitope-specific CD8$^+$ T-cell populations were determined by sequencing.

Results: A 2F-positive population was rarely observed under our culture and staining conditions. The wt-positive CD8$^+$ T-cell populations had a diverse TCR repertoire, but the TCR repertoires in dual-positive CD8$^+$ populations were highly restricted. In the dual-positive CD8$^+$ T-cell populations, most clonotypes used the TRBV4-1 and TRBJ2-7 gene segments for the TCR β-chain and the TRAV8-3 and TRAJ40-1 for the TCR α-chain. The CDR3 region of the TCR β-chain showed little variation.

Conclusion: These results provide an example of restricted TCR repertoire in a specific CTL response against the escaping epitope. We speculate that impairment of antigen presentation in escaping viruses may underlie the restricted repertoire.

AIDS 2009, **23**:651–660

Keywords: CD8$^+$ T cells, HIV infection, human leukocyte antigen, T-cell epitope, T-cell receptor repertoire

Introduction

Cytotoxic T lymphocytes (CTLs) play a very important role in counteracting HIV-1 infection [1–3]. However, the hallmark of HIV-1 infection is the incomplete response of CTLs. It is crucial to understand the molecular mechanisms of antigen presentation and recognition in the context of immunopathogenesis of HIV-1.

[a]Division of Infectious Diseases, Advanced Clinical Research Center, [b]Department of Infectious Diseases and Applied Immunology, Research Hospital, [c]Research Center for Asian Infectious Diseases, The Institute of Medical Science, The University of Tokyo, Tokyo, Japan, and [d]Division of Molecular Immunology, Institute of Microbiology, Chinese Academy of Sciences, Beijing, China.

Correspondence to Aikichi Iwamoto, MD, Professor, Division of Infectious Diseases, Advanced Clinical Research Center, The Institute of Medical Science, The University of Tokyo, 4-6-1 Shirokanedai, Minato-ku, Tokyo 108-8639, Japan.

Tel: +81 3 5449 5359; fax: +81 3 6409 2008; e-mail: aikichi@ims.u-tokyo.ac.jp

* E.M. and A.K.-T. contributed equally to the writing of this article.

Received: 28 August 2008; revised: 12 November 2008; accepted: 25 November 2008.

DOI:10.1097/QAD.0b013e32832605e6

ISSN 0269-9370 © 2009 Wolters Kluwer Health | Lippincott Williams & Wilkins

CTLs use T-cell receptors (TCRs) to recognize peptide-major histocompatibility complex (MHC) (pMHC) complexes presented on the surface of the infected cells. Error-prone reverse transcription of HIV-1 can result in amino acid substitutions in the cognate peptides. Mutated viruses may acquire selective advantage against CTLs and become dominant escape variants [4,5]. Substitution of amino acid residues critical for binding to MHC molecules [6,7] or TCR recognition [8,9] can result in escape mutants. Even substitution of the amino acids flanking the cognate peptides can result in escape mutants by altering the peptide processing and decreasing the number of pMHC molecules that are recognized by CTLs [10–14].

Amino acid substitutions in the HIV-1 escape mutants may be stereotypic in different individuals sharing the same MHC haplotypes [12,15]. We previously reported that HIV-1 with a stereotypic substitution from Y [Nef138-10(wt)] to F [Nef138-10(2F)] at the second position in an immunodominant HLA-A*2402(A24)-restricted CTL epitope in the Nef protein (Nef138-10) has a strong selective advantage in A24-positive patients [12]. There is a high prevalence of A24 in the Japanese population, and unprotected sexual contact has transmitted the 2F substitution among A24-positive individuals throughout Japan. How HIV-1 with the Nef138-10(2F) substitution could have a selective advantage in A24-positive patients remains an enigma, as we detected vigorous $CD8^+$positive T-cell ($CD8^+$) responses not only against Nef138-10(wt) but also against Nef138-10(2F) in PBMCs from A24-positive patients [12].

In this study to explore the effector side, we stimulated cultured $CD8^+$ T cells obtained from A24-positive, HIV-1-infected patients and stained them simultaneously with two A24 tetramers that presented either Nef138-10(wt) or Nef138-10(2F). We then sorted the epitope-specific $CD8^+$ T cells that recognized wild-type or 2F or both and analyzed the TCR repertoire.

Materials and methods

Study patients

We analyzed CTL response in peripheral blood mononuclear cells (PBMCs) from seven patients who were HIV-1 infected and HLA-A*2402 positive. Patients were randomly selected among patients participating in an ongoing HIV-1-immunopathogenesis study at an HIV outpatient clinic affiliated with the Institute of Medical Science, the University of Tokyo. All but one of the seven subjects (S15) were antiretroviral therapy naive. The study was approved by the internal review board of the Institute of the Medical Science of the University of Tokyo (No. 11-2), and all patients provided informed consent.

Cell media and study reagents

Culture media and supplements were purchased from Sigma (St Louis, Missouri, USA) except as otherwise noted. R(−) medium consisted of RPMI 1640 supplemented with 100 U/ml penicillin, 100 μg/ml streptomycin, 10 mmol/l 4-(2-hydroxyethyl)-1-piperazineethanesulfonic acid (HEPES) and 2 mmol/l L-glutamine. R10 medium was R(−) medium supplemented with 10% heat-inactivated fetal calf serum (FCS).

Synthetic peptides Nef138-10(wt) (RYPLTFGWCF), Nef138-10(2F) (RFPLTFGWCF) were purchased from Sigma-Genosys (Ishikari-shi, Hokkaido, Japan).

Enzyme-linked immunosorbent spot assay

Enzyme-linked immunosorbent spot (ELISPOT) assay was performed using freshly prepared PBMCs (5×10^4 cells) as previously described [16].

In-vitro stimulation with Nef138-10 peptides

PBMCs were divided into two aliquots and prepared for in-vitro stimulation with Nef138-10 peptides as previously described [17]. To prepare antigen-presenting cells, PBMCs of 5×10^5 patients were pulsed with 10 nmol/l Nef138-10(wt) or Nef138-10(2F) at 37°C for 1 h. Cells were washed twice with R10, then cultured in R10 with 1×10^6 fresh autologous PBMCs and 4×10^6 irradiated (3300 rads) PBMCs from healthy individuals. After 4 days, recombinant human IL-2 (rIL-2; Wako, Osaka, Japan) was added to 50 U/ml. The culture was continued for 2 weeks, with medium changed every 3–4 days (R10 with 50 U/ml rIL-2).

Preparation of major histocompatibility complex-class I tetramers presenting Nef138-10(wt) or Nef138-10(2F)

Soluble forms of pMHC molecules were produced in CV-1 cells using a Sendai virus (SeV) vector expression system and purified from the supernatant as described previously [18]. After affinity purification, pMHC molecules were biotinylated with BirA enzyme (Avidity, Aurora, Colorado, USA) and purified by gel filtration chromatography with a Superdex 200 column (GE Healthcare, Piscataway, New Jersey, USA).

Biotinylated Nef138-10(wt)/HLA-A24 (Nef138-10(wt)/A24) or Nef138-10(2F)/HLA-A24 (Nef138-10(2F)/A24) complexes were tetramerized with allophycocyanin (APC)-labeled or phycoerythrin-labelled streptavidins (Invitrogen, Eugene, Oregon, USA), respectively

Flow cytometry and sorting of cytotoxic T lymphocytes

Stimulated PBMCs were incubated at 37°C for 15 min in the presence of Nef138-10(wt)/A24-APC or Nef138-10(2F)/A24-PE or both. The final concentrations of Nef138-10(wt)/A24-APC and Nef138-10(2F)-PE in monomer pMHC were 11 and 8 μg/ml, respectively.

Cells were washed with fluorescence-activated cell sorter (FACS) buffer (PBS supplemented with 2% FCS and 0.02% NaN_3) and further stained with either fluorescein isothiocyanate (FITC)-labeled or Pacific Blue-labeled anti-CD8 T-cell antibodies (BD Pharmingen, San Jose, California, USA) or anti-TCR β-chain V gene 4-1 antibodies (TRBV4-1) (Beckman Coulter, Fullerton, California, USA) at 4°C for 30 min. Cells were then washed with FACS buffer and fixed by a 20-min incubation at reverse transcriptase in the dark in PBS containing 1% paraformaldehyde.

Flow cytometry was performed using a FACS Calibur (Beckton Dickinson, Franklin Lakes, New Jersey, USA) and FACS Aria (Beckton Dickinson). Flowjo ver. 6.4.7 (Tree Star, Ashland, Oregon, USA) was used for the analysis. For cell sorting, the cells were stained in R10 medium instead of FACS buffer, stained with propidium iodide to remove dead cells, and sorted without fixation using a FACS Aria.

T-cell receptor repertoire determination

Total RNA was extracted from sorted T cells using an RNeasy Micro Kit (Qiagen, Venlo, The Netherlands). We synthesized full-length cDNA by anchored RT-PCR using the super switching mechanism at 5′-end of the RNA transcript (SMART) PCR cDNA synthesis kit (TakaraBio, Otsu, Shiga, Japan), according to the manufacturer's protocol, with the switching mechanism at the 5′ end of RNA transcript. To amplify the variable, diversity, and joining regions of the TCR genes, the second PCR was done with the first primer and the reverse primers specific for the TCR α or β constant region: the 3′ T-cell receptor α chain constant region (TRAC) primer (5′-GGCAGACAGACTTGTCACTG GATTTAGAG-3′) or the 3′ T-cell receptor β chain constant region (TRBC) primer (5′-TGACCC CACTGTGCACCTC-3′), respectively. Reaction conditions in the second PCR were as follows: 94°C for 1 min; 25 extension cycles of 94°C for 30 s, 55°C for 30s, 72°C for 1 min; and a final extension at 72°C for 7 min. Reaction products from the second PCR were purified with Wizard PCR preps DNA purification System (Promega, Madison, Wisconsin, USA) and subcloned into pGEM-T East vector (Promega).

DNA sequencing was performed using an ABI Prism dye terminator cycle sequencing ready reaction kit (Applied Biosystems, Foster City, California, USA) on a Perkin-Elmer ABI-377 sequencer. Designation of TCR genes follows the international immunogenetics (IMGT) nomenclature [19]. We defined the CDR3 region of the TCR β-chain as the region from aa 104 in T-cell receptor Vβ (TRBV) to aa 7 in TRBJ and the CDR3 region of the TCR α-chain as the region from aa 105 in TRAV to aa 11 in TRAJ.

Results

Nef138-10-specific response in HLA-A*2402+ patients

We analyzed PBMCs from seven A24-positive patients with chronic HIV-1 infection. All patients except one (S15) were naive to antiretroviral treatment. The median viral load was 6700 copies/ml (range, 120–24000 copies/ml), and the median CD4 T-cell count was 437 cells/μl (range, 278–807 cells/μl).

Using the plasma samples obtained closest to the following analyses, we confirmed that plasma viruses had stereotypically Nef138-10(2F) in all the patients analyzed (Fig. 1). Nef138-10-specific responses of $CD8^+$ T cells were analyzed by IFN-γ ELISPOT assay. Although the magnitude of specific response varied substantially among the samples, all showed a response to Nef138-10(wt) and Nef138-10(2F) (Fig. 1).

Tetramer dual-staining of Nef138-10-specific $CD8^+$ T cells

After 2-week culture in the presence of 10 nmol/l Nef138-10(wt) or Nef138-10(2F) peptides, PBMCs were stained with Nef138-10(wt)/A24-APC [Tet(wt)] or Nef138-10(2F)/A24-PE [Tet(2F)] or both. Using cultured cells from patient S15, we examined whether dual staining fractionated the Nef138-10-specific cells more precisely than single staining. Single stainings with Tet(wt) and Tet(2F) stained 9.8% (Fig. 2a) and 6.2% (Fig. 2b) of S15 $CD8^+$ T cells, respectively, after stimulation with Nef138-10(wt). In dual staining with the two tetramers, 7.2% of S15 $CD8^+$ T cells were in the Tet(wt)-positive/Tet(2F)-positive (dual-positive) fraction and 4.2% were in the Tet(wt)-positive/Tet(2F)-negative (wt-positive) fraction (Fig. 2c). Similarly, after Nef138-10(2F) stimulation, single staining of $CD8^+$ T cells from patient S15 with Tet(wt) and Tet(2F) stained 6.0 (Fig. 2d) and 6.1% of cells, respectively (Fig. 2e). With dual staining, 3.3% of S15 $CD8^+$ T cells stimulated with Nef138-10(2F) were dual-positive, and 2.2% were wt-positive.

These preliminary pilot experiments suggested that dual staining could fractionate dual-positive and wt-positive cells regardless of the peptide used for stimulation. Under the culture and staining conditions we used, the Tet(wt)-negative/Tet(2F)-positive (2F-positive) population was minimal. As we could fractionate dual-positive and wt-positive cells under these conditions, we inferred that the $CD8^+$ T cells in each fraction had different affinities for pMHC, that is, Tet(wt) or Tet(2F).

To examine the TCR repertoire in different fractions, we cultured PBMCs from seven patients and stained the cells with both Tet(wt) and Tet(2F) (Fig. 2g–m). In cells from patient O14, only Tet(wt)-positive cells were more than

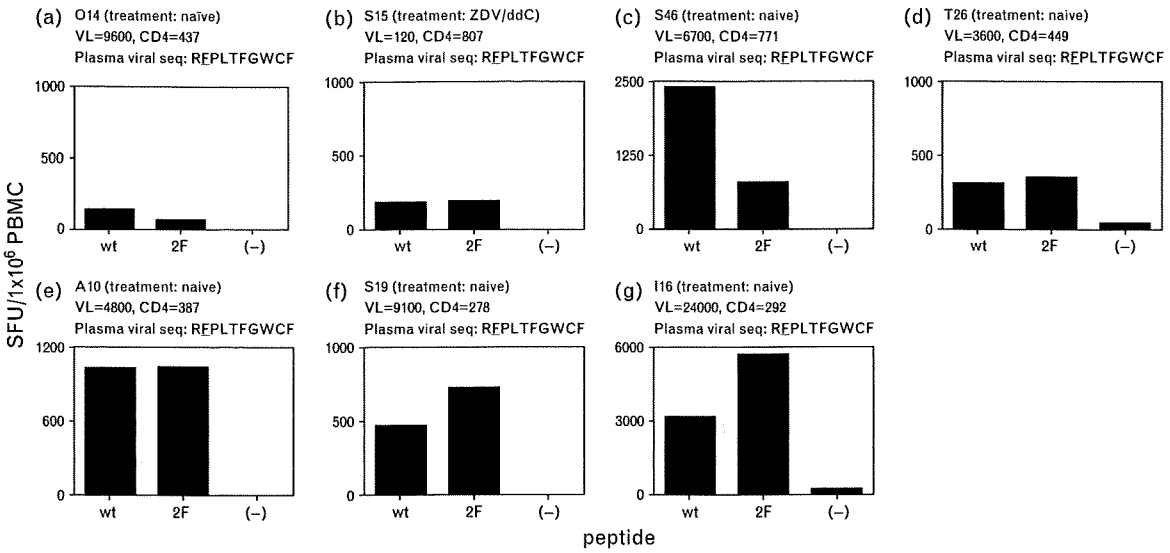

Fig. 1. Study patients and Nef138-10-specific responses. Peripheral blood mononuclear cells (PBMCs) from seven patients were stimulated with Nef138-10(wt) (RYPLTFGWCF), Nef138-10(2F) or mock. Spot-forming units (SFUs)/1 × 10^6 PBMCs after stimulation are shown in subparts a–g. The viral load (VL) and CD4 T-cell count (CD4) of each patient are shown. All patients had HLA-A*2402 and their plasma viruses had Nef138-10(2F) mutation (RFPLTFGWCF).

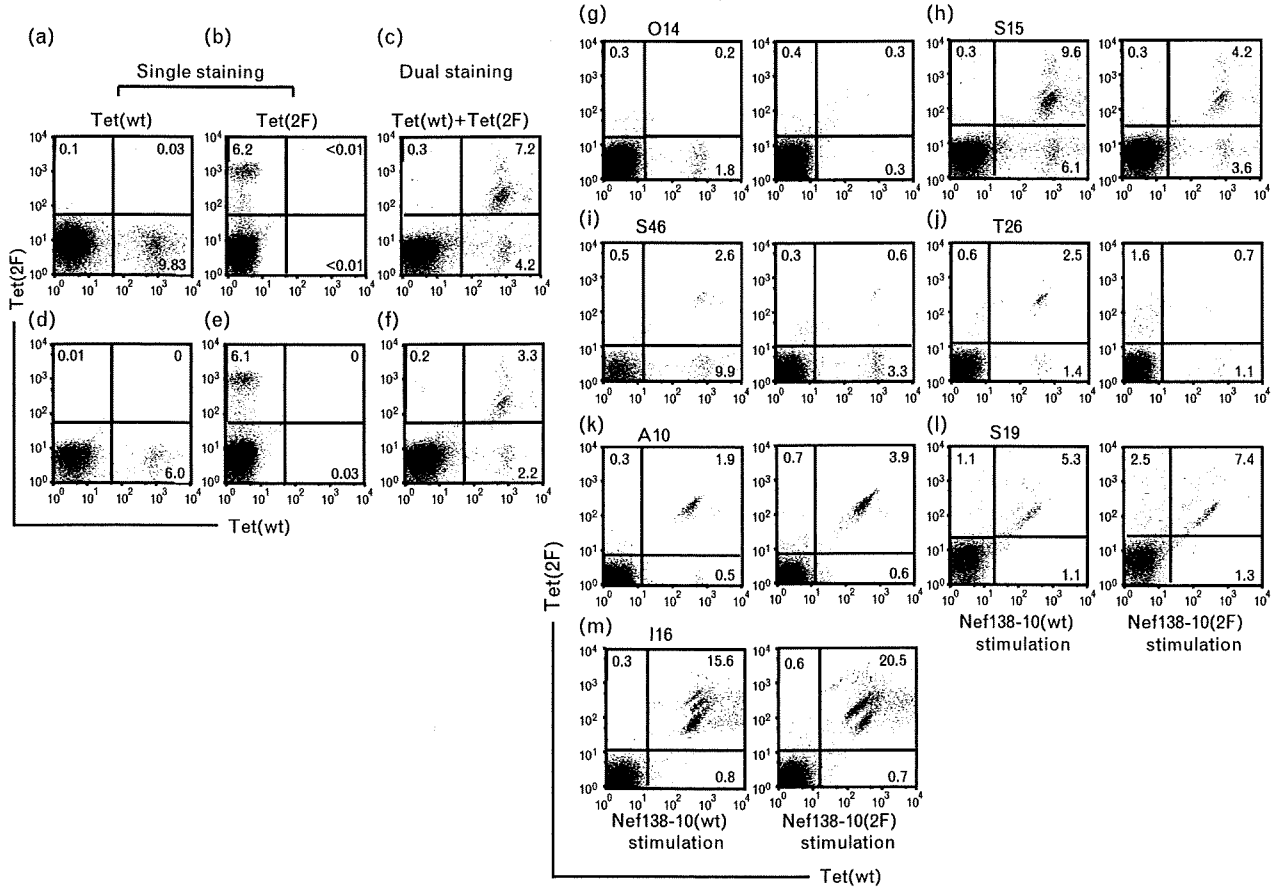

Fig. 2. Tetramer staining of peripheral blood mononuclear cells stimulated with Nef138-10(wt) or Nef138-10(2F). Peripheral blood mononuclear cells (PBMCs) from patient S15 were stimulated with Nef138-10(wt) (a, b, c) or Nef138-10(2F) peptides (d, e, f). Cells were stained with Nef138-10(wt)/A24-APC-tetramer [Tet(wt)] (a, d) or Nef138-10(2F)/A24-PE-tetramer [Tet(2F)] (b, e) or both (c, f) as described in 'Materials and Methods'. Cultured PBMCs from seven patients were stained with both Tet(wt) and Tet(2F) (g–m) including an S15 sample from a different culture (h). Dot plots are gated on $CD8^+$ T cells. Numbers refer to the percentages of gated cells in each quadrant.

1% of the population after Nef138-10(wt) stimulation (Fig. 2g). Nef138-10(2F) failed to induce specific $CD8^+$ T cells in cultures derived from patient O14. In cultures from patients S15, S46, and T26, both dual-positive and wt-positive $CD8^+$ T-cell populations were detected (Fig. 2h–j). Although Nef138-10-specific $CD8^+$ T cells were induced with both Nef138-10(wt) and Nef138-10(2F), the former induced higher expansion of cells derived from patients S15, S46, and T26. However, in cultures from patients in A10, S19, and I16, higher expansion of Nef138-10-specific $CD8^+$ T cells was induced with Nef138-10(2F) stimulation than with Nef138-10(wt) stimulation (Fig. 2k–m). In cultures derived from these three patients, the great majority of cells after stimulation were dual-positive.

Only in patient T26 was the 2F-positive population distinguished clearly from the dual-positive population, though the 2F-positive population showed lower fluorescent intensity (phycoerythrin) than did the dual-positive population (Fig. 2j). With a 1000-fold increase, from 10 nmol/l to 10 μmol/l, in concentration of Nef138-10(wt) and Nef138-10(2F) peptides used for stimulation, we observed expansion of 2F-positive $CD8^+$ T cells from other patients (data not shown).

T-cell receptor repertoire of wt-positive and dual-positive $CD8^+$ T-cell populations

Cell sorting showed substantial diversity among the study patients in the TCR repertoire of the wt-positive population of CD8 cells induced with Nef138-10(wt) (Fig. 3). The TCR repertoire also varied slightly according to the peptides used for stimulation. We observed 7.0 ± 2.2 different TCR β-chain clonotypes per individual after stimulation with Nef138-10(wt) peptides, compared with 6.3 ± 3.5 different clonotypes per individual after stimulation with Nef138-10(2F) peptides. Patients differed in whom β-chain V gene (TRBV) was most frequently used after Nef138-10(wt) stimulation. After Nef138-10(2F) stimulation, TRBV7-9 was the most common TCR β-chain clonotype seen in each of the three patients analyzed (patients S15, S46, and T26) (Fig. 4a).

In the dual-positive population, we observed only 3.3 ± 1.5 clonotypes per patient following Nef138-10(wt) stimulation and 1.8 ± 1.0 different clonotypes per patient following Nef138-10(2F) stimulation (Fig. 3). There were significantly fewer clonotypes in the dual-positive populations than in the wt-positive populations, regardless of stimulation conditions. Following Nef138-10(wt) stimulation, the mean number of clonotypes observed in the dual-positive population was 3.3 ± 1.6, compared with 7.0 ± 2.2 in the wt-positive population ($P = 0.01$, Mann–Whitney *U*-test). Following Nef138-10(2F) stimulation, the mean numbers of clonotypes in the dual-positive and wt-positive populations were 1.8 ± 1.0 and 6.5 ± 3.5, respectively ($P = 0.048$).

Notably, TRBV usage was highly restricted in the dual-positive population in all patients examined. TRBV4-1 was used in 84% of the analyzed clones, irrespective of stimulating peptides, and was the major TRBV in all clones except in those from patient I16 (Figs 3 and 4a). At the time of our analysis, the major TCR β-chain gene segments in patient I16 were TRBV15 and TRBV10-3; however, further studies using frozen PBMCs obtained from this patient 2 years earlier showed TRBV4-1/TRBJ2-7 to be the most frequently used clonotype (data not shown).

TCR β-chain joining gene (TRBJ) usage was more restricted in the dual-positive population compared with the wt-positive population, irrespective of the peptides used for stimulation (Fig. 3). Ninety-four percent of the dual-positive population in the analyzed clones used TRBJ2-7, whereas in the wt-positive population, TRBJ usage was more diverse (Fig. 4a). The CDR3 TCR β-chain region was also conserved in the dual-positive $CD8^+$ T-cell population. The length of the CDR3 region ranged from 12–16 amino acids in the dual-positive population, compared with 10–19 amino acids in the wt-positive population (Fig. 3). The CDR3 region had a length of 13 amino acids in 63% of the dual-positive population induced by Nef138-10(wt) stimulation and in 68% stimulated with Nef138-10(2F). More than 70% of the dual-positive clones using TRBV4-1/TRBJ2-7 conserved proline at the variable–diversity junction (fifth position of CDR3) and glycine and isoleucine at the diversity–joining junction. Surprisingly, the most frequent CDR3 amino acid sequence was identical in clones from three patients (S15, S46, and S19) (Fig. 4b). However, the nucleotide sequences were not identical, and distinctive clones were isolated from patients S15 and S46 (Fig. 4b), clearly indicating that the same TCR β-chain arose from different recombination events.

To examine the TCR α-chain diversity in a population with a highly restricted TCR β-chain repertoire, we analyzed TCR α-chain sequences in the dual-positive population after Nef138-10(2F) stimulation in PBMCs from patients S46, A10, and S19. In these three patients, the dual-positive population used TCR α-chain variable gene (TRAV) 8-3 and joining gene (TRAJ) 40 (Fig. 4c). The CDR3 region was highly conserved in length, ranging from 14 to 15 amino acids and clones using TRAV8-3/TRAJ40-conserved proline at the sixth position. Thus, the dual-positive $CD8^+$ T-cell population showed a highly restricted repertoire in both TCR α and β chains, including the CDR3 sequence.

T-cell receptor Vβ usage in the dual-positive $CD8^+$ T-cell population *in vivo*

The analyses described above showed that dual-positive $CD8^+$ T-cell populations expanded *in vitro* had a highly restricted TCR repertoire; that is, TRBV4-1/TRBJ2-7 and TRAV8-3/TRAJ40. We hypothesized that selection

wt-positive CD8+T cells

	Nef138-10(wt)-stimulation						Nef138-10(2F)-stimulation					
	TRBV	CDR3		TRBJ	Freq. (%)	No.Seq	TRBV	CDR3		TRBJ	Freq. (%)	No.Seq
O14	27	CASS TGG	EQF	2-1	(38)	104clones						
	11-2	CASS SDTGTGGLI	NGYT	1-2	(35)							
	19	CASS IGAGTGT	PTLY	1-3	(9)							
	5-5	CASS SEVL	AEAF	1-1	(7)							
	6-1	CASS DIGRGV	HEQY	2-7	(6)							
	6-1	CAS RIDGSSY	NEQF	2-1	(2)							
	7-2	CASS LGGGGT	DTQY	2-3	(1)							
	7-9	CASS LVEGTG	WEQF	2-1	(1)							
	2	CA RRTSGRE	TQYF	2-5	(1)							
S15	10-2	CASS ESIGGRDNN	QPQH	1-5	(43)	23clones	7-9	CASS SYYRSG	NTIY	1-3	(22)	27clones
	28	CASSLSTGRGT	YEQY	2-7	(26)		28	CASS LSTGRGT	YEQY	2-7	(22)	
	7-9	CASS SYYRSG	NTIY	1-3	(9)		10-2	CASS ESIGGRDNN	QPQH	1-5	(19)	
	4-1	CASS QGWFAASV	QPQH	1-5	(4)		6-5	CTSV PAVRSQRDRGQ	ETQY	2-5	(7)	
	4-1	CASS PTAGI	YEQY	2-7	(4)		5-4	CASS LTG	ETQY	2-5	(7)	
	6-1	CASS DIGQGAI	EQY	2-7	(4)		12-3	CASS LGQGE	ETQY	2-5	(7)	
	30	CAW GNPGLNT	GELF	2-2	(4)		10-1	CAKR AGGAT	DTQY	2-3	(3)	
	11-2	CASS YDRS	YEQY	2-7	(4)		6-1	CASS DIGQGA	IEQY	2-7	(3)	
							7-9	CASS LDETGG	YEQY	2-7	(3)	
							7-9	CASS ARAGTSGA	GELF	2-2	(3)	
S46	5-5	CASS LEQFT	DEQY	2-7	(32)	25clones	7-9	CASS LRDSVP	ETQY	2-5	(48)	19clones
	7-9	CASS LRDSVP	ETQY	2-5	(24)		5-5	CASS LEQFTD	EQY	2-7	(42)	
	7-9	CASS SWDTG	ELF	2-2	(20)		25-1	CAS SASGQQP	YEQY	2-7	(10)	
	6-1	CASS DAQTGTVLN	YGYT	1-2	(8)							
	25-1	CAS SASGQQP	YEQY	2-7	(8)							
	5-1	CASS LELST	GELF	2-2	(4)							
	4-2	CASS PPGL	NTQY	2-3	(4)							
T26	7-9	CASS LRDRVP	ETQY	2-5	(57)	30clones	7-9	CASS LRDRVP	ETQY	2-5	(50)	30clones
	6-1	CASS DFGQGD	EAF	1-1	(23)		6-1	CASS DFGQGD	EAF	1-1	(20)	
	21	CATW DMSSYN	SPLH	1-6	(12)		6-1	CASS FRPGLAV	TGELF	2-2	(10)	
	6-1	CASS FRPGLAV	TGELF	2-2	(6)		7-8	CASS LIVQGW	YEQY	2-7	(10)	
							21	CATW DMSSYN	SPLH	1-6	(6)	
							27	CASS AGYN	EQF	2-1	(3)	

Dual-positive CD8+T cells

	Nef138-10(wt)-stimulation						Nef138-10(2F)-stimulation					
	TRBV	CDR3		TRBJ	Freq. (%)	No.Seq	TRBV	CDR3		TRBJ	Freq. (%)	No.Seq
S15	4-1	CASS PGQ[illegible]	YEQY	2-7	(28)	29clones	4-1	CASS PGQ[illegible]	YEQY	2-7	(53)	30clones
	4-1	CASS QLA[illegible]V	YEQF	2-1	(28)		4-1	CASS QLA[illegible]V	YEQF	2-1	(40)	
	4-1	CASS RTSG[illegible]S	YEQY	2-7	(18)		4-1	CASS QLSG[illegible]T	YEQY	2-7	(7)	
	4-1	CASS PTA[illegible]	YEQY	2-7	(14)							
	4-1	CASS PTSG[illegible]T	YEQY	2-7	(10)							
	4-1	CASS QLSG[illegible]T	YEQY	2-7	(3)							
S46	4-1	CASS PGQ[illegible]	YEQY	2-7	(92)	24clones	4-1	CASS PGQ[illegible]	YEQY	2-7	(100)	26clones
	5-1	CASS LELST	GELF	2-2	(8)							
T26	4-1	CASS GT[illegible]	YEQY	2-7	(90)	31clones	4-1	CASS QTSG[illegible]T	YEQY	2-7	(100)	31clones
	4-1	CASS QTSG[illegible]T	YEQY	2-7	(6)							
	20	CSAG RTS[illegible]	YEQY	2-7	(4)							
A10	4-1	CASS PTQ[illegible]	YEQY	2-7	(98)	45clones	4-1	CASS PTQ[illegible]	YEQY	2-7	(100)	50clones
	24	CATS DPDREVE	ETQY	2-5	(2)							
S19	4-1	CASS PGQ[illegible]	YEQY	2-7	(90)	48clones	4-1	CASS PGQ[illegible]	YEQY	2-7	(95)	55clones
	5-4	CASS FGSNL	YEQY	2-7	(6)		4-1	CASS HTT[illegible]L	YEQY	2-7	(5)	
	4-1	CASS HTT[illegible]L	YEQY	2-7	(4)							
I16	15	CATS RASG[illegible]T	YEQY	2-7	(68)	31clones	10-3	CAIS ESTGLAVF	YEQY	2-7	(77)	30clones
	10-3	CAIS ESTGLAVF	YEQY	2-7	(20)		4-1	CASS PQK[illegible]	YEQY	2-7	(16)	
	4-1	CASS PQK[illegible]	YEQY	2-7	(10)		15	CATS RASG[illegible]T	YEQY	2-7	(7)	
	28	CASS LMKAGDG	YGYT	1-2	(2)							

Fig. 3. T-cell receptor β-chain repertoire of Nef138-10/A24-tetramer wt-positive and dual-positive CD8$^+$ T-cell populations. CDR3 amino acid sequence, TRBV and TRBJ usage and relative frequency of Nef138-10-specific CD8$^+$ T cells stimulated with Nef138-10(wt) or Nef138-10(2F) are shown. Data from Tet(wt)+/Tet(2F)−(wt-positive) population are shown in the upper column, and data from Tet(wt)+/Tet(2F)+ (dual-positive) are shown in the lower column. Numbers in parentheses indicate frequency (%) of each clonotype. TCRs detected in both Nef138-10(wt) and Nef138-10(2F) stimulation in the same patient are highlighted with gray bars. The TCR clonotype conserved among patients is highlighted with yellow bars. The consensus amino acid sequences, occurring in more than 70% clones in TRBV4-1/TRBJ2-7, are indicated with red. The designation of TRBV and TRBJ follows Folch's nomenclature [19].

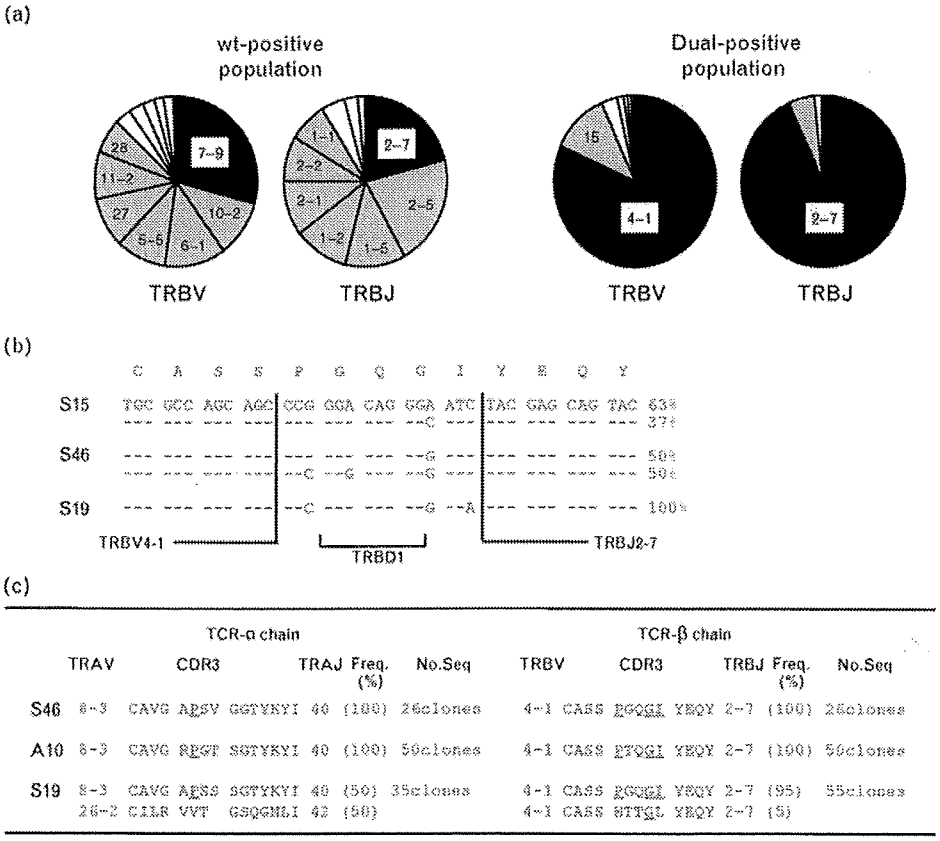

Fig. 4. Characteristics of T-cell receptor β-chain of Nef138-10/A24-tetramer wt-positive and dual-positive CD8$^+$ T-cell populations. Frequencies of TRBV and TRBJ gene usage in CD8$^+$ T cells stimulated with Nef138-10(wt) (Fig. 3) were calculated and shown in a graph. Tet(wt)+/Tet(2F)− (wt-positive)(left) and Tet(wt)+/Tet(2F)+ (dual-positive) (right) populations are shown. The most frequent genes are indicated by black shading, and genes found in more than 5% of the population are indicated by gray shading (a). Nucleotide sequence of CDR3-coding region (CASSPGQGIYEQY) in S15, S46, and S19 was aligned (b). CDR3 amino acid sequence, TRAV, TRAJ, TRBV, and TRBJ usage, and relative frequency of Tet(wt)+/Tet(2F)+ (dual-positive) population in S15, S46, and S19 are shown. Numbers in parenthesis indicate frequency (%) of each clonotype. The consensus amino acid sequences are underlined (c).

could be occurring during in-vitro stimulation by peptides. In order to examine whether the dual-positive population also used TRBV4-1 primarily *in vivo*, frozen PBMCs were thawed and stained with Tet(wt), Tet(2F), and anti-TRBV4-1 antibodies (Fig. 5). PBMCs from patients S15 and T26 had too few dual-positive cells to assess; however, in PBMCs from patients A10 and S19, more than 95% of the dual-positive CD8$^+$ T-cell population were TRBV4-1 positive.

Discussion

Error-prone reverse transcriptase creates the genetic diversity of HIV-1 and serves as an effective means for the virus to evade immune surveillance. Considering the plasticity and hypervariable nature of HIV-1, stereotypic amino acid substitution in the CTL epitope is an enigma that might provide clues to understanding the difficulties encountered in developing effective vaccines for HIV-1. One might predict that point mutations affecting the HIV-1 anchor residues would remove its ability to bind to an MHC heavy chain, resulting in a CTL epitope incapable of eliciting specific CTL response [4]. However, substituted CTL epitopes such as Nef138-10(2F) show the escape phenotype, yet bind to MHC molecules almost as efficiently as the wild-type epitope, with the interaction eliciting strong CD8$^+$ T-cell response [12,13,20].

In this study, we examined the TCR repertoire of CD8$^+$ T cells responding to wt [Nef138-10(wt)] and mutant [Nef138-10(2F)] epitopes. By tetramer dual-staining of A24-positive PBMCs stimulated *in vitro* from HIV-positive patients, we were able to examine two CD8-positive T-cell populations: wt-positive and dual-positive populations. In three patients, the CD8$^+$ T cells could be differentiated according to their relative affinity to Nef138-10(2F)/A24 tetramers (Figs 2 and 3); we designated as 'wt-positive' the population with lower affinity to Nef138-10(2F)/A24 tetramers. Regardless of

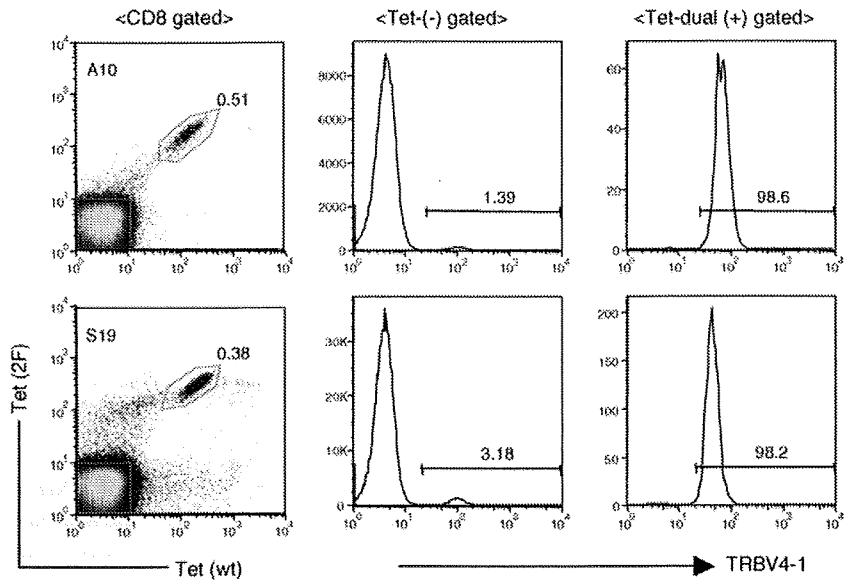

Fig. 5. TRBV4-1 expression in Nef138-10/A24-tetramer dual-positive population *in vivo*. Frozen peripheral blood mononuclear cells from two patients (A10, S19) were stained with Tet(wt) and Tet(2F), anti-CD8 (Pacific Blue), and anti-TRBV4-1(FITC). Tet(wt)+/Tet(2F)+ (dual-positive) and tetramer negative [Tet-(−)] populations are gated. Expression of TRBV4-1 in each population is shown in histogram. FITC, fluorescein isothiocyanate.

which peptide was used for stimulation, the TCR repertoire of the wt-positive population was similar in each patient.

An unexpected finding was that the dual-positive $CD8^+$ T-cell population grown *in vitro* had a highly restricted TCR repertoire compared with the wt-positive $CD8^+$ T-cell population, which showed substantial diversity. Furthermore, the dual-positive $CD8^+$ T-cell population *in vivo* also appeared to have a restricted CTL repertoire in which TRBV4-1 was the predominant clonotype.

Patient I16 appeared to be an exception; in the dual-positive $CD8^+$ T-cell population from this patient, TRBV15 and TRBV10-3 were the major TCR β-chain gene segments. At the time of the study, patient I16 had been followed as an HIV-infected patient in our clinic for at least 8 years, longer than any other study patient. Analysis using frozen PBMCs from patient I16 showed that TRBV4-1/TRBJ2-7 had been the most frequently used clonotype 2 years earlier (data not shown).

In this study, the 2F-positive population was distinguished clearly only in patient T26. Expansion of 2F-positive $CD8^+$ T cells was observed in PBMCs from some of the other patients only following stimulation with much higher peptide concentrations (data not shown). We speculate that 2F-positive $CD8^+$ T cells may require higher amounts of antigen for stimulation and proliferation.

One apparent limitation of our study is that we did not formally prove that the wt single-positive cells are not dual-specific for wt and unknown epitopes, including variant Nef138-10 other than Nef138-10(2F). Although sequencing results showed that the plasma viruses were all Nef138-10(2F) (Fig. 1), we could stimulate and expand $CD8^+$ T cells not only with Nef138-10(2F), but also with Nef138-10(wt) peptides. Our interest is not in the hidden additional specificity of the wt-positive population, but in their relative inability to bind the pMHC to which they must have been exposed *in vivo*. The dual-positive population with higher affinity to Nef138-10(2F)/A24 tetramers had a restricted TCR repertoire. Notably, the patients were viremic even in the presence of CTLs that had a higher affinity against the cognate 'mutant' CTL epitope, Nef138-10(2F)/A24, yet were still able to recognize the cognate 'wt' CTL epitope.

Our data suggest that mutation at the second residue (P2) in the HLA-A24-binding epitope influences T-cell recognition. P2 is the anchor residue of the HLA-A24-binding peptide and dips into the B pocket, forming a hydrogen bond with H70 in the HLA-A24 molecule [21]. A single amino acid substitution from Y to F at a secondary anchor position has been shown to modify the overall conformation of the HLA-A2-restricted HIV Gag-SL9 peptide [22]. However, our recent studies suggest that Y139F substitution in Nef138-10 does not cause a drastic change in pMHC structure (unpublished observation).

Dong *et al.* [23] reported the close correlation between Vβ13.2 usage and long-term nonprogression in four HLA-B8-positive patients. Vβ13.2-positive CTLs were widely reactive to possible escape mutants. In our study, the patients were randomly selected. The relationship between the restricted TCR repertoire and the patient's prognosis is not known, yet we do know that two of the